Project co-funded by the European Commission within the FP7 (2007–2013)

Grant agreement no.: 308630

I-PAN

INNOVATIVE POPLAR LOW DENSITY STRUCTURAL PANEL

Project type: Collaborative Project

Start date of project: 1st October 2012 Duration: 36 months

D6.3 – Report on the elaborated engines and software for blending technology

WP n° and title	WP6 – Blending technologies
WP leader	IMAL
Responsible Author(s)	UMIL: Fabio Scotti
Contributor(s)	UMIL
Planned delivery date	M30 (March 2015)
Actual delivery date	M30 (March 2015)
Reporting period	RP2

Add an "x" in the box representing the dissemination level of the deliverable, as in the DoW

Dissemination Level		
PU	Public	**x**
PP	Restricted to other programme participants (including the Commission Services)	
RE	Restricted to a group specified by the consortium (including the Commission Services)	
CO	Confidential, only for members of the consortium (including the Commission Services)	

Document information

Abstract

This deliverable includes a description of the acquisition setups and image-processing algorithms developed to monitor the blending process. Two different acquisition setups have been introduced. One setup acquires 3-D images from free-falling strands, and it can perform a granulometric analysis of the strands before they enter the blending process. The other setup acquires and analyzes 2-D images from the conveyor belt and it was designed to check the strands after they have gone through the blending process. Two processing algorithms have been designed and tested for this last setup. The first one uses segmentation to analyze the granulometry of the strands, while the second approach provides a qualitative analysis of the strands.

Keywords

Strands blending, 3D vision setup, 2D vision setup, granulometric analysis, qualitative strand size analysis

Authors

Editor(s)	Vincenzo Piuri, Fabio Scotti, Sergio Damas, Andrea Valsecchi
Contributors	UMIL, ECSC
Peer Reviewers	IMAL

Document history

Version	Date	Reviewed paragraphs	Short description
0.1	*24/02/15*	*All*	*First draft*
0.2	*10/03/15*	*All*	*Second draft*
0.3	*24/03/15*	*All*	*Release for peer review*
1.0	*31/03/15*	*All*	*Final version for the EC*

* Abbreviations of editor/contributor name

Table of Contents

LIST OF ABBREVIATIONS AND DEFINITIONS 6

1 Introduction 7

1.1 Analysis of previous solutions 7
1.1.1 Segmentation based approaches 7
1.1.2 Methods that avoid segmentation 8
1.1.3 Previous solutions for the three-dimensional granulometry 9

2 Analysis of the strands before entering into the blender 10

2.1 Layout of the vision-based system 10

2.2 Techniques to analyze free-falling strands 10
2.2.1 Camera calibration and acquisition 10
2.2.2 Segmentation 11
2.2.3 Point matching and 3D triangulation 12
2.2.4 3D normalization 12
2.2.5 Granulometric analysis 14
2.2.6 Analysis of the thickness of the strands 14

2.3 Experiments 19
2.3.1 Acquisition setup 19
2.3.2 Acquisition procedure 19
2.3.3 Robustness to environmental conditions 19
2.3.4 Working range 19
2.3.5 Accuracy of granulometric analysis 20

3 Analysis of the strands after the blending process 23

3.1 Layout of the vision-based system 23

3.2 Granulometry analysis based on segmentation 25
3.2.1 Image enhancement 26
3.2.2 Particle segmentation 27
3.2.3 Particle selection 27

3.3 Quality analysis in frequency domain 28
3.3.1 Description of the method 29

3.4 A method to generate realistic synthetic images 32

3.5 Experiments 33
3.5.1 Analysis of the segmentation-based method 33
3.5.2 Analysis of the frequency-based method 36

4 Conclusions 39

5 References 40

LIST OF FIGURES

Figure 1 – Schema of the controlled space where the acquisition system for monitoring the blending process should be deployed. 10

Figure 2 – Layout of the acquisition system (side view) 11

Figure 3 – Layout of the acquisition system (frontal view) 11

Figure 4 – Layout of the acquisition system (top view) 12

Figure 5 - Estimation of the strand rotation using the plane interpolating the 3D point cloud of the strand. The roll and pitch angles can be computed by considering the displacements of the plane along the axes 13

Figure 6 - Strand captured with a frontal acquisition. It is not possible to observe its thickness. 15

Figure 7 - Strand captured with a sideways orientation. In some parts of the image the thickness is visible, but in others the strand is almost blended with the background. 16

Figure 8 - Strand captured in a close-to-sideways position. 16

Figure 9 - Strand captured with about 5 degree orientation with respect to the camera optical axis, using a uniform blue background 17

Figure 10 - Set of rows extracted from the image (a) and corresponding tomography (b) 17

Figure 11 - Estimation of strands' thickness using a 3-D profilometer 19

Figure 12 - Example of 3-D profilometer 19

Figure 13 - Examples of strands captured with the Camera A: (a,b) strands compliant to the reference size provided by the manufacturing industry; (c,d) strands non-compliant to the reference size. The strands in (c,d) have a lower width with respect to the strand 20

Figure 14 - Layout of the acquisition system A (side view). The arrow represent the direction in which the mattress moves. 23

Figure 15 - Layout of the acquisition system A (top view). The arrow represent the direction in which the mattress moves. 24

Figure 16 – Layout of the acquisition system B (side view). The arrow represent the direction in which the mattress moves. 24

Figure 17 – Layout of the acquisition system B (top view). The arrow represent the direction in which the mattress moves. 25

Figure 18 - Blocks used to perform the segmentation. 26

Figure 19 - Particle identification steps. 26

Figure 20 - Examples of the different steps followed to obtain the final granulometry. a) the initial image. b) result of the Laplacian filter. c) result of the contrast enhancement. d) result of the edge elimination. e) result after clustering. f) result after binarization. g) final segmentation. h) segmenation superimposed on the original image. i) analysis of the granulometry, which presents boxplots and histograms for four measurements: major axis, minor axis, equivalent diameter and area. 28

Figure 21 - Examples of the bands used to produce the histogram 30

Figure 22 - Histogram extracted from an image with resolution 1200 × 1600, which presents including real strands of low quality. Top-left, original image. Top-right, magnitude of the Fourier transform. Bottom, the final histogram displayed as a log-log plot 31

Figure 23 - Comparison of histograms obtained from images with strands of diverse qualities. 32

Figure 24 - A synthetic mattress from different angles. 33

Figure 25 - Examples of the images used in the tests. First column shows images of the real mattress, second column presents synthetic images. The size of the strands present in the images increases from top to bottom. 34

Figure 26 - Histograms obtained for the minor axis of real images: a) image containing only big strands, b) image containing both small and big strands, c) image containing only small strands. The results show how, as the proportion of small strands present in the image grows, the approach detects less strands with a big minor axis and more with a small minor axis. 35

Figure 27 Examples of the images of real wood particles used in the tests. The quality of the strands, according to the target specifications indicated for the project, increases from left to right and from top to bottom. 37

Figure 28 - Examples of the noisy images containing salt and pepper noise, which simulates device noise, (first column) and gaussian blur, which simulates the noise caused by a dirty lens or an out of focus problem, (second column). 38

LIST OF TABLES

Table 1 - Real strand sizes, classified into bins (%) 21

Table 2 - Computed strand sizes, classified into bins (%) 21

Table 3 - Classification error according to the strand width 22

Table 4 - Results, in mm, obtained using mattress images. 35

Table 5 - Results in mm obtained using artificial images. 36

Table 6 - Mean confusion matrices obtained for real images. 37

Table 7 - Results obtained for noisy images. 38

LIST OF ABBREVIATIONS AND DEFINITIONS

DoW	Description of Work
EC	European Commission
PM	Project Manager
PMQP	Project Management and Quality Plan
PMB	Project Management Board
PR	Peer reviewer
TMB	Technical Management Board
QM	Quality Manager
DM	Deliverable Manager
WP	Work Package

1 INTRODUCTION

The objective of this document is to present the vision-systems and algorithms developed to monitor the performance of the blending technologies. The vision-systems perform real-time monitoring to analyze the blending effects on the strands. Both two-dimensional and three-dimensional setups are employed to study and prevent possible strand damages, which, in turn, can result in a better use of the resources and raw materials and in the obtaining of lighter and less expensive panels.

The main goal of the developed systems is to study the granulometry, i.e., the particle size distribution, of the wood strands employed in the production of OSB panels. This study is important since the size of the strands is directly related to the quantity of resin necessary to produce the final panel.

To study and prevent possible strand damages, it will be necessary to estimate the measures of the strand before entering in the blending engine, and after resin spraying. During the development of the project, the two measures that emerged as more important were the length and width. Hence, the systems have been accordingly optimized to obtain a good performance. In addition, some techniques based on 3D-reconstruction have been studied to provide an estimation of the variation trend in the strands' thickness.

This document introduces two acquisition setups and three methods developed to perform a real-time monitoring that controls the blending effects on the strands and helps estimating the optimal amount of resin.

The first acquisition method is based on a two-view acquisition setup that obtains 3-D images from free-falling strands. This setup is designed to be used before the wood strands start the blending process. In addition, a method that analyzes the 3-D images and performs a granulometric analysis of the strands is proposed.

The second acquisition setup obtains the images from a top-view of the conveyor belt. This setup has been designed to be used after the wood strands have gone through the blending process. Two methods have been developed to analyze the images produced using this setup. The first one uses an optimized segmentation method to perform a granulometric analysis of the strands present on the surface of the mattress. The second one performs a qualitative analysis of the strands, by studying the Fourier transform of the image.

The deliverable is organized as follows. The remaining of this section analyzes previous approaches that have performed image-based granulometric studies. Section 2 shows the techniques developed to analyze the images of free-falling strands. Section 3 introduces the methods created to study the images of the strands after the blending process. Section 4 presents the conclusions.

1.1 ANALYSIS OF PREVIOUS SOLUTIONS

The analysis of granulometry using vision systems has been studied for a long time. However, the performance of the methods in literature has varied widely and the solutions offered in the market are not general [1]. Reviews on image processing methods for the particle size measurement in different applicative scenarios are presented in [2], [3], [4], [5] and [6]. In this section, some of the most relevant approaches are analyzed. The study is divided in three parts; the first part considers traditional approaches that analyze 2-D images by segmenting them. After that, the techniques that study 2-D images avoiding segmentation are evaluated. The last part studies those approaches that use a 3-D approach.

1.1.1 SEGMENTATION BASED APPROACHES

In general, vision-based systems employ a single camera and follow a two-step process in order to estimate the size distribution of the objects present in the image: first the image is segmented to locate the objects that appear in it; after that, the properties of the identified objects are evaluated and aggregated to estimate their distribution. In order to obtain high confidence on the obtained results it is important to measure as many objects as possible [7].

The approach based on two steps has been followed in a variety of fields. Including biology, mining, panel production, and a long etcetera.

In the field of biology, several approaches have been followed. Theera-Umpon et al. [8] used a non-homothetic granulometric filter to estimate the blood cell proportions corresponding to different cell-age categories. Their approach relaxes previous models providing a model that is conceptually better for counting problems in which particles have random shape and size. Zapater et al. [9] analysed images of the corneal endothelium, the inner layer of the human cornea, using successive structural openings. They were able to obtain different cumulative distribution functions, like mean, standard deviation, kurtosis and skewness. Comparing these distributions to those obtained by groups of control, they managed to discover changes in cell morphology. Iftikhar et al. [10] introduced a technique particularly designed for the measuring of blood cells called CLIC (Capture Largest Included Circles), which uses a parametrized segmentation algorithm capable of capturing the largest possible circles in an object boundary.

Other area with intense research to determine particle size distributions, is the classification of powders. In this field, Boschetto and Giordano [11] proposed a versatile digital image procedure consisting on image calibration, enhancing and clustering capable of retrieving 2D properties of powder particles. The method is able to calculate significant size and shape information or powder particles. In addition, Mazzoli and Favoni [12] analysed Scanning Electron Microscopy images using classical image processing techniques to characterize morphology, size and size distribution of wood dust particles obtained from different wood types.

This problem has also been studied in industrial environments. For instance, in mining industry many approaches have been proposed. Williams et al. [13] use different techniques, like mathematical morphology processing, edge detection, thresholding, region growing, region merging or region splitting, to characterize the shape distributions of bulk material. Salehizabeh and Sadeghi [14] used traditional image-processing techniques like opening operations, watershed or area boundary to calculate particle size distributions of stone fragments in a mining factory. Koh et al. [15] developed a technique to improve the results of granulometry on images with many overlapping particles. Their approach captures multiple images with different illumination conditions, which helps to segment particles.

With regard to the analysis of wood particles, one of the first studies was introduced by Greiner and Link [16]. They statistically evaluated dimensional features extracted from images of ring-cut flakes in order to categorize the strands into two quality classes. Later, Nishimura et al. [17] analyzed the influence of temperature on the quality of the obtained wood particles. This analysis is based on shape characteristics extracted from strands images. The acquisition setup uses a CCD camera and two light sources. Grayscale images with a resolution of 1299x1016 pixels were obtained.

1.1.2 METHODS THAT AVOID SEGMENTATION

However, segmentation represents the most important source of estimation errors when the setup is not controlled [18]. For instance, when the particles are superimposed, or the illumination is not correct. In addition, the segmentation of a complex and densely populated scene, which may include superimposed elements, is typically a computationally intensive task. For this reason, other researchers have proposed methods that avoid segmentation.

Zadorozny et al. [19] used two transformation techniques, Fourier analysis and scale-space decomposition, to estimate particle size distribution. In particular, these techniques were applied to the analysis of oil sand images, both from simulated artificial data and real video images, demonstrating the feasibility of the two approaches. Ledda et al. [20] applied a similar approach to the analysis of a polymer called “polyimide”. In particular, they extract different parameters from the Fourier transform and the patter spectrum and analyse their correlation with the particle size distribution, obtaining a set of parameters that provides interesting information.

Following a different approach, Ljungqvist et al. [21] used mathematical morphological opening operations to estimate the particle size distribution of food pellets for aquaculture. Their results show that it is possible to estimate diameter, length and area of the pellets, from an image of piled disordered pellets.

Using a different approach, Ferrari et al. [18] presented a method based on the application of neural networks image analysis algorithms. This method estimates features from local regions centered in every pixel and exploits them using neural networks. In order to compute the features input images is convolved with Gaussian kernels. After training each pixel is classified according to the probability to belong to a specific size class.

1.1.3 PREVIOUS SOLUTIONS FOR THE THREE-DIMENSIONAL GRANULOMETRY

This section presents the few works in the literature which propose methods for the three-dimensional granulometry of particles.

A laser scanner is used in the method described in [22] for monitoring the quality and analyzing the size of wood chips. The laser scanner is used to compute a three-dimensional model of the objects by projecting a laser beam on the chips passing on the conveyor belt. The displacement of the laser line is then used to reconstruct the three-dimensional information. Classification methods based on regression techniques and Support Vector Machine (SVM) are used to classify the chips. However, the fact that this method requires multiple images captured at different times in order to compute a three-dimensional model makes it not suited for analyzing falling strands.

A method based on a stereoscopic image acquisition setup is described in [23] for measuring the size distribution of crystals suspended in the water. The acquisition setup is composed by a single camera and two mirrors, which are place around the flow of the particles. A segmentation algorithm is used to extract the particles in the two captured images, then the corresponding particles are matched and a three-dimensional model is computed. The size of the particles is computed from the three-dimensional model. However, in order to function correctly the particles must not overlap, and have similar axes sizes.

The method described in [24] proposes a shape-from-shading algorithm with the purpose of computing the three-dimensional model of granular substances, and then using the model to estimate the size distribution. However, this method is only suited for particles with a smooth surface.

2 ANALYSIS OF THE STRANDS BEFORE ENTERING INTO THE BLENDER

This Section describes the techniques used for analyzing the strands before entering into the blender. In particular, hardware acquisition setups, image acquisition procedures and image processing algorithms have been designed and implemented in order to estimate the size distribution of the strands as they are free falling into the blender.

2.1 LAYOUT OF THE VISION-BASED SYSTEM

The acquisition system for monitoring the blending process is based on a two-view acquisition system placed in a position where it is possible to capture images of free falling strands. In order to perform the monitoring, the strands should fall in a controlled space, with a plexiglass window that allows the camera to capture images of the strands, and led bars used to illuminate the field of view, as shown in Figure 1. If necessary, flux deflectors should be used to deviate the falling path of the strands to the controlled space.

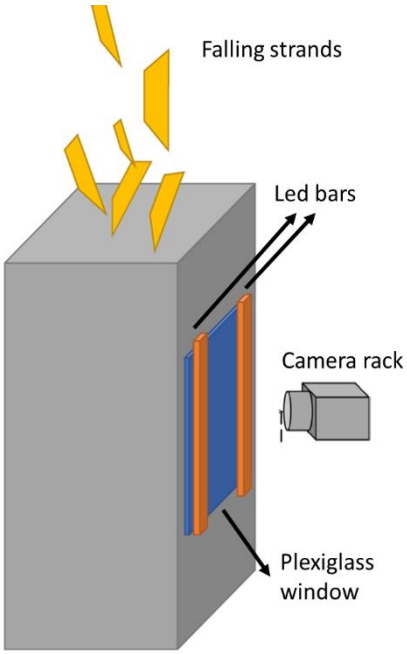

Figure 1 – Schema of the controlled space where the acquisition system for monitoring the blending process should be deployed.

The layout of the acquisition system for monitoring the blending process is shown in Figure 2 (side view), Figure 3 (frontal view) and Figure 4 (top view).

2.2 TECHNIQUES TO ANALYZE FREE-FALLING STRANDS

In this section the method used for analyzing the strands and estimating their size distribution is described. In particular, the approach is composed by five steps:

1. camera calibration and acquisition;
2. segmentation;
3. matching of the points and 3D triangulation;
4. 3D normalization;
5. granulometric analysis and size estimation.

2.2.1 CAMERA CALIBRATION AND ACQUISITION

First, two CCD cameras are synchronized using a trigger mechanism, and then calibrated by performing the acquisitions of a chessboard in multiple different positions and orientations. Then, a corner detector is used

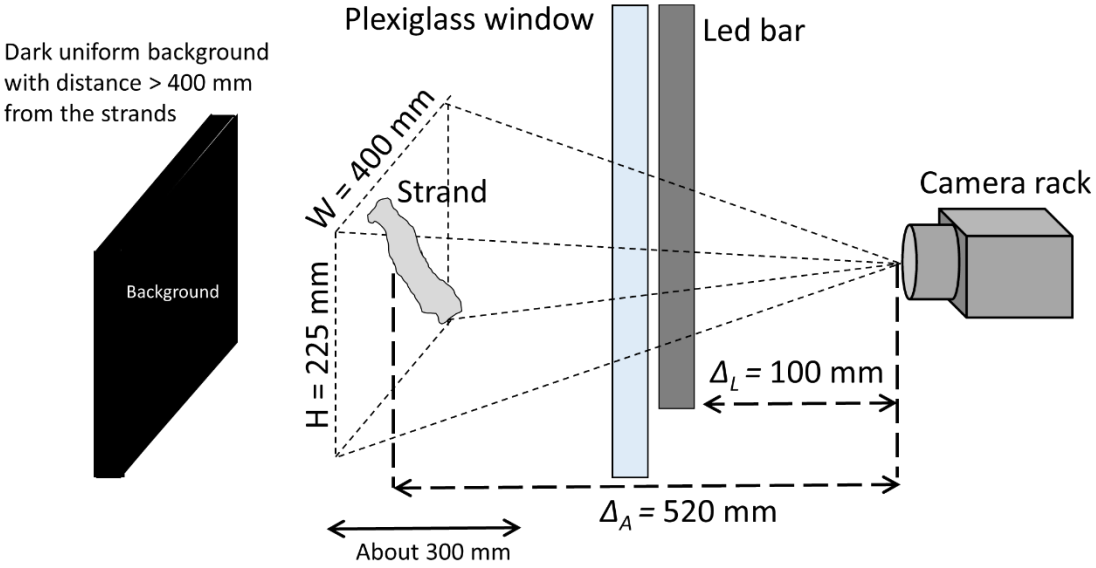

Figure 2 – Layout of the acquisition system (side view)

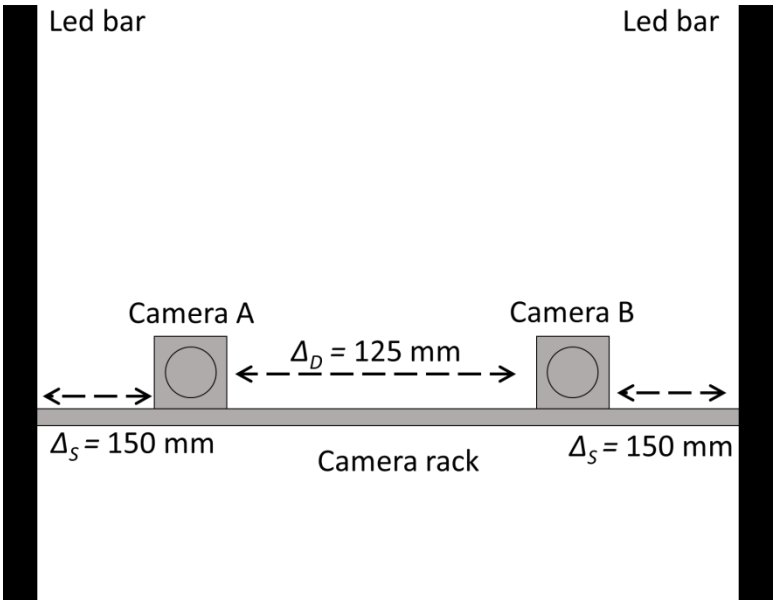

Figure 3 – Layout of the acquisition system (frontal view)

to extract the corners of the chessboards in the images. The intrinsic, extrinsic, and homography parameters of the cameras and the two-view acquisition system are computed by using the methods proposed in [25, 26, 27].

A two-view acquisition is then performed as the strand is falling, and two led bars are used to illuminate the strands. Each acquisition is composed by the images I_A and I_B, respectively captured using Camera A and Camera B (Figure 4).

2.2.2 SEGMENTATION

The captured images are binarized by using the following formula:

$$M_A(x,y) = \begin{cases} 1 \text{ if } R_A(x,y) > Y_A(x,y) \text{ and } B_A(x,y) < Y_A(x,y) \\ 0 \text{ otherwise} \end{cases}$$

Where M_A is the binary segmentation mask, R_A and B_A are the red and blue channels of the image I_A, and Y_A is the grayscale image computed from I_A.

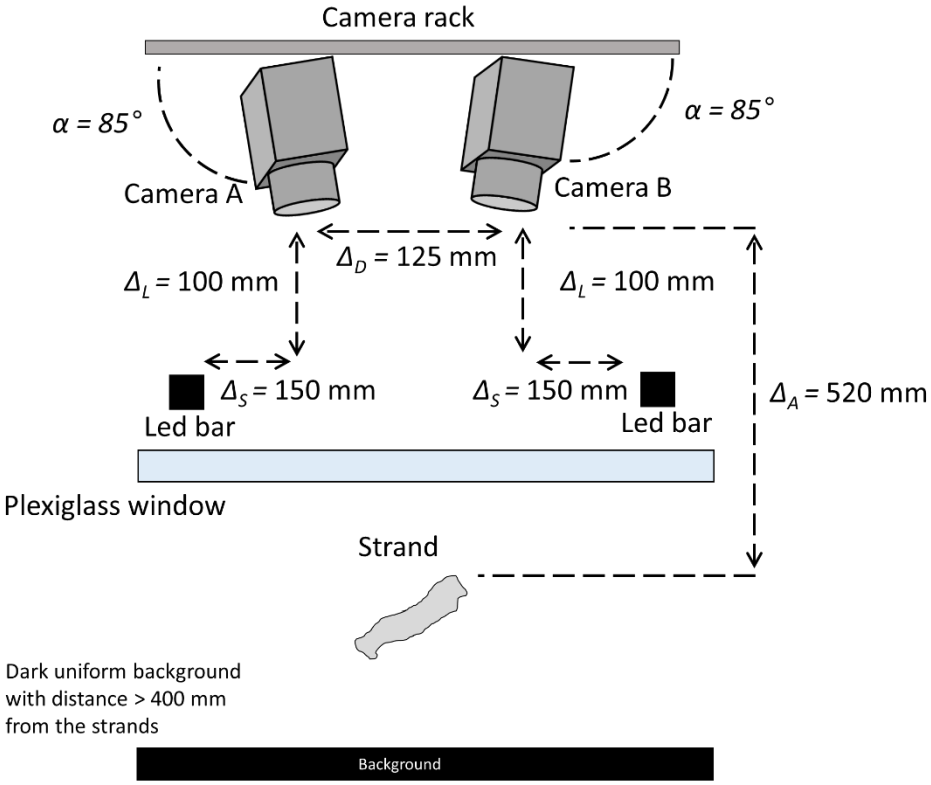

Figure 4 – Layout of the acquisition system (top view)

Then the images is processed using morphological operators, in particular a morphological opening operation, followed by a closing operation, is performed. The operator is a disk-shaped structuring element with size $s_{th} = 5$. The same segmentation process is performed on the image I_B.

2.2.3 POINT MATCHING AND 3D TRIANGULATION

This section describes the proposed method for the computation of the three-dimensional shape of the particle borders.

As a first step, an edge detector is used to extract the edges of the Regions of Interest (ROI) of the two images M_A and M_B. Then, the edges are analyzed considering a single y coordinate at a time: if the same number of points is present in the two images, for each coordinate, then the points are considered matched:

$$|a(x,j) = |b(x,j)| \rightarrow (a,b) \in P \quad \forall\, 1 < j < Y$$

Where $|\cdot|$ represents the cardinality of the set, P is the matched point set, and Y is the vertical size of the image.

The three-dimensional position of each matched pair of points is then computed by using the intrinsic and extrinsic parameters of the acquisition setup, computed previously. In particular, the triangulation function is applied to determine the three-dimensional coordinate of a point, given the two-dimensional coordinates of the two matching points in the two captured images [27]. A three-dimensional spike filter, described in [28], is used to remove possible outliers, with the results of obtaining the three-dimensional point cloud (X, Y, Z).

2.2.4 3D NORMALIZATION

The three-dimensional normalization step has the purpose of compensating the orientation of the strand in the three-dimensional space, in order to minimize the displacement of the point cloud along the z axis. The result of this step is a point cloud lying on the XY plane.

As a first step, a procedure based on a linear interpolation is used to fit a plane (X_p, Y_p, Z_p) through the obtained three-dimensional point cloud of the particle borders. A plane fitting operation is used since the strands are almost flat, and a plane can represent the strand with a good level of approximation.

Then, in order to compute the roll and pitch angles, the displacements of the plane along the three axes are considered as the catheti of two right triangles (**Figure 5**). By using this representation, the pitch and roll angles can be computed using trigonometric formulas.

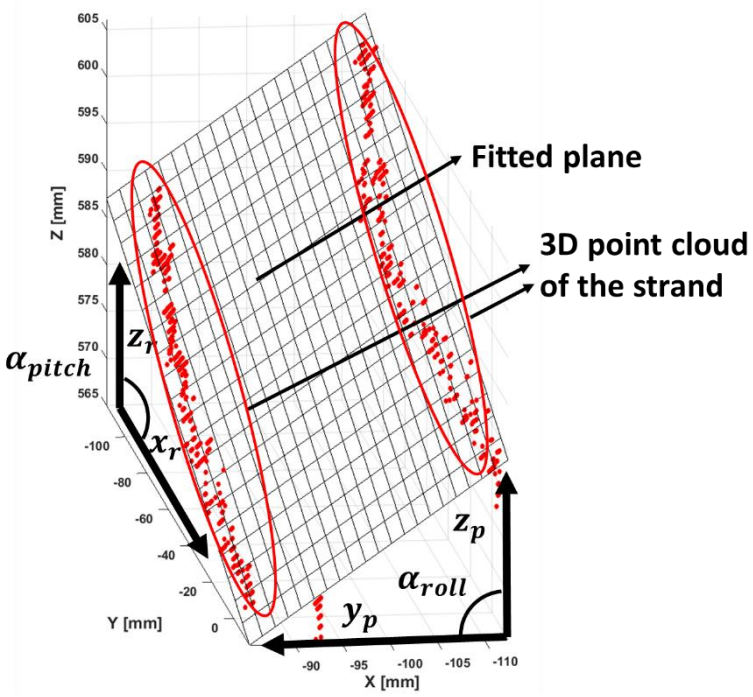

Figure 5 - Estimation of the strand rotation using the plane interpolating the 3D point cloud of the strand. The roll and pitch angles can be computed by considering the displacements of the plane along the axes

In particular, in order to compensate for the roll angle, first the displacements of the point cloud of the plane along the x and y axes are computed using the following formula:

$$\Delta x_r = \max X_p - \min X_p$$
$$\Delta z_r = \max Z_p - \min Z_p$$

and the hypotenuse a_r is computed using the Pythagorean theorem. Then, the roll angle α_{roll} can be estimated using the following formula:

$$\alpha_{roll} = \sin^{-1} \frac{\Delta z_r}{a_r}$$

Then, the rotation matrix for the angle α_{roll} is computed as:

$$R_{roll} = \begin{bmatrix} \cos \alpha_{roll} & 0 & \sin \alpha_{roll} \\ 0 & 1 & 0 \\ -\sin \alpha_{roll} & 0 & \cos \alpha_{roll} \end{bmatrix}$$

and the rotation is applied to all the points of the three-dimensional point cloud of the particle borders (X, Y, Z), in order to obtain the point cloud $(X_{roll}, Y_{roll}, Z_{roll})$:

$$\begin{bmatrix} X_{roll} \\ Y_{roll} \\ Z_{roll} \end{bmatrix} = R_{roll} \begin{bmatrix} X \\ Y \\ Z \end{bmatrix}$$

In order to compensate for the pitch angle, first the displacement of the point cloud of the plane along the y and z axes are computed using the following formula:

$$\Delta y_p = \max Y_p - \min Y_p$$
$$\Delta z_p = \max Z_p - \min Z_p$$

Then, the hypotenuse a_p is computed using the Pythagorean theorem. The pitch angle α_{pitch} is then computed using the following formula:

$$\alpha_{pitch} = \sin^{-1} \frac{\Delta z_p}{a_p}$$

The rotation matrix corresponding to the angle α_{pitch} is computed as follows:

$$R_{pitch} = \begin{bmatrix} \cos \alpha_{pitch} & 0 & \sin \alpha_{pitch} \\ 0 & 1 & 0 \\ -\sin \alpha_{pitch} & 0 & \cos \alpha_{pitch} \end{bmatrix}$$

The rotation is applied to the point cloud $(X_{roll}, Y_{roll}, Z_{roll})$, obtained after the correction of the roll angle, in order to obtain the point cloud $(X_{pitch}, Y_{pitch}, Z_{pitch})$, which is the point cloud representing the particles borders lying on the XY plane:

$$\begin{bmatrix} X_{pitch} \\ Y_{pitch} \\ Z_{pitch} \end{bmatrix} = R_{pitch} \begin{bmatrix} X_{roll} \\ Y_{roll} \\ Z_{roll} \end{bmatrix}$$

2.2.5 GRANULOMETRIC ANALYSIS

The granulometric analysis, in which the size of the strands is estimated, is computed by projecting the point cloud $(X_{pitch}, Y_{pitch}, Z_{pitch})$ on the image plane. In particular, an image G is created by assigning 1 to the points in the image where the x and y coordinates correspond to a point in the three-dimensional point cloud, as expressed by the formula:

$$G(x,y) = \begin{cases} 1 \text{ if } (x,y) \in (X_{pitch}, Y_{pitch}) \\ 0 \text{ otherwise} \end{cases}$$

Then, the convex hull of the image binary image G is computed, and the major and minor axes are extracted. The size of the strand is estimated by considering the computed axes as its length and width.

2.2.6 ANALYSIS OF THE THICKNESS OF THE STRANDS

This section analyzes the problem of measuring the thickness of the wood strands. The analysis of this dimension is difficult because of the constraints imposed by the estimation of the characteristics that have emerged as critical during the development of the project, i.e., the strand's length and width. In particular, for the captured area necessary to correctly measure them, the thickness of the strand is too close to the limit of the image resolution. Hence, using the acquisition setups developed in this section and in Section 3 it is not possible to obtain accurate measurements.

Using the acquisition system that has been introduced in Section 2, nonetheless, it could be possible to estimate a variation trend in the strand's thickness. However, in order to have useful data that permits to achieve this objective, it would be necessary to acquire, directly in the plant, as many strand images as possible. Even though this makes the problem very difficult, we have studied some techniques that could determine if the strands' thickness is deriving towards a value outside the stipulated limits.

It is possible to consider two different approaches for the problem of measuring the strand thickness:

1. Monitoring the trend of the strand thickness;
2. Directly and accurately measuring the strand thickness on each strand.

2.2.6.1 Methods to monitor the trend

In the first case, it is not necessary that the measure performed on each strand represents an actual thickness value in mm, nor the measure needs to be precise. It is sufficient that, for each strand, it is performed a measure which is related to the strand thickness. By observing how such measure change over time, it is possible to infer if the thickness of the strands is deviating from a reference value. The relation between such reference value and the obtained measure can be established by observing the behavior of the system when the strands are known to have a thickness compliant to the reference value. Moreover, by aggregating the performed measures on multiple strands, it is possible to obtain more precise measures.

The advantage of the first approach is that no accurate measurement is required and, if no real-time requirements are present, the trend estimation can be made more precise by aggregating the measures performed on a greater number of strands, captured on a longer time frame.

The second approach, based on directly measuring the strand thickness for each particles, requires an actual metric measurement (in mm) for the thickness of each strand. Moreover, the measurement needs to be more precise as it cannot be aggregated over multiple strands.

If an acquisition setup based on cameras is used to perform the monitoring of the blending process, as those describe in this deliverable, measuring the strand thickness is a very challenging task. In fact, the thickness is very small (< 1 mm) compared to the length and width of the strands, and a subpixel analysis could be necessary. Moreover, only particular orientations of the strands at the moment of the acquisition allow the thickness to be visible, with the consequence that such analysis is possible on only a small subset of the images.

After an experimental evaluation, it was observed that there are three possible orientations of the strand at the moment of the acquisition, which influence how the thickness is visible:

1. Strand in a frontal position (the surface is oriented perpendicularly to the camera optical axis);
2. Strand in a sideways position (the surface is oriented in parallel to the camera optical axis and at the center of the acquisition area);
3. Strand with close-to-sideways position (the surface is oriented with an angle about 5 degrees with respect to the camera optical axis).

In the case of a strand captured with a frontal acquisition, the thickness is not visible, as shown in Figure 6.

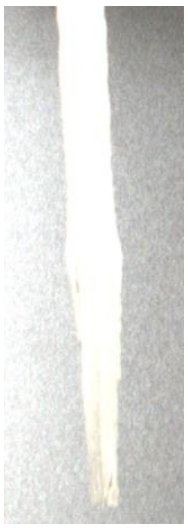

Figure 6 - Strand captured with a frontal acquisition. It is not possible to observe its thickness.

On the other hand, if the strand is captured with a sideways orientation with respect to the cameras, even if the thickness is visible, the strand can be easily confused with the background, since only a very limited portion of the surface is visible, as shown in Figure 7. In this case, it would be difficult to correctly segment the image. Moreover, the irregularities of the strand shape could prevent such measure to be performed on all the length of the strand.

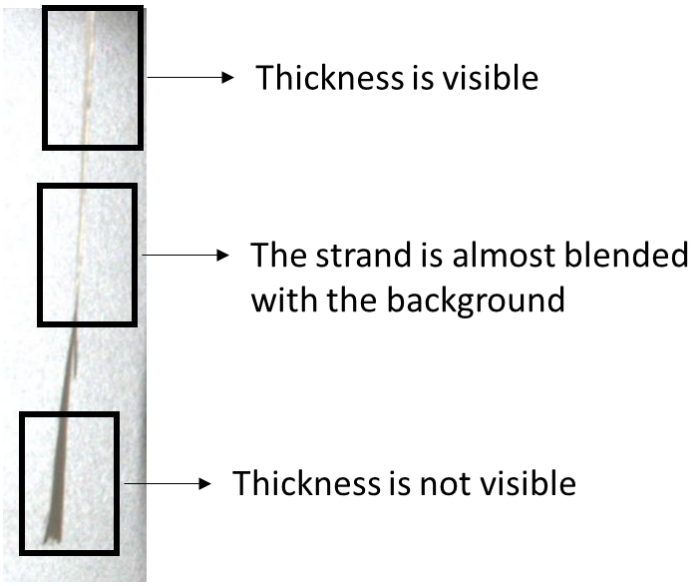

Figure 7 - Strand captured with a sideways orientation. In some parts of the image the thickness is visible, but in others the strand is almost blended with the background.

In the case of a strand captured with close-to-sideways position, the thickness can be visible, as shown in Figure 8. However, small variations in the orientation of the strands, as well as their color, could result in changes in the image which would prevent the thickness to be visible. For these reason, the analysis of the strand thickness could be performed on only a small subset of the strands.

Then, in order to analyze this kind of images, it is necessary to compute a three-dimensional model of the strand, so that it is possible to estimate the angle of the strand with respect to the camera optical axis. Then, it would be possible to extract only the images that have about a 5 degrees angle of orientation with respect to the camera optical axis. Moreover, it would be necessary to segment the area of the strand corresponding to the thickness information.

If the segmented area corresponding to the strand thickness is extracted, it would be possible to process it using image processing algorithms, by either computing an abstract measure, which could be aggregated over multiple strands and used to estimate the trend in the thickness, or using the information related to the camera calibration in order to compute a direct measure of the strand thickness.

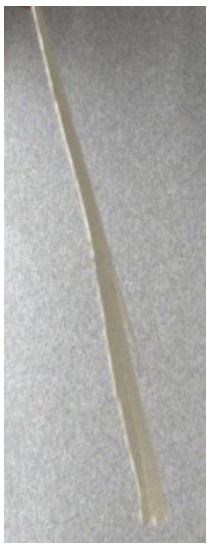

Figure 8 - Strand captured in a close-to-sideways position.

In particular, we captured the strands with about a 5 degree angle with respect to the camera optical axis, using a uniform blue background in order to simplify the segmentation process (Figure 4).

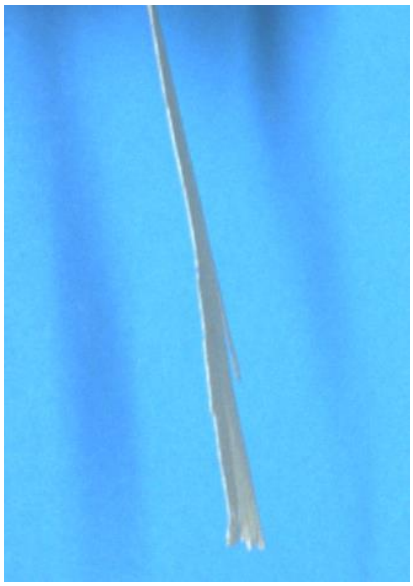

Figure 9 - Strand captured with about 5 degree orientation with respect to the camera optical axis, using a uniform blue background

It is possible to observe that, in the case of a strand oriented in this manner, the thickness of the strand is directly illuminated and the corresponding region of the image has greater intensity values. We then extracted from the image a set of 9 rows, equally spaced along the length of the strand, and performed the tomography (Figure 5).

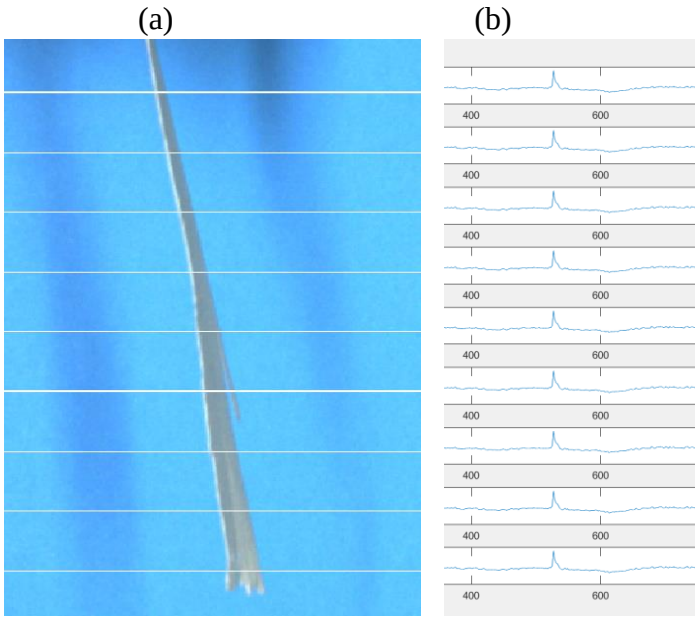

Figure 10 - Set of rows extracted from the image (a) and corresponding tomography (b)

Then, the thickness region for each row is selected as the 99.5% percentile of the intensity values in each row. The thickness of the strand (in pixels) is then computed as the average thickness for each extracted row.

It is then necessary to convert the measure from pixels to millimeters. In particular, we performed a set of acquisition of a ruler, placed perpendicularly with respect to the camera optical axis, at different distances from the camera. Then, we manually computed the ratio between 100 mm, as indicated by the ruler, and the corresponding size in pixel on the image. In this way, we obtained a look-up table with the conversion coefficients from pixels to mm, for different distances from the camera.

Then, to compute the distance of the strand from the camera, we perform a two-view acquisition and the corresponding three-dimensional reconstruction, using the vision setup and the methods described in Section 2.1 (Layout of the vision-based system) and Section 2.2 (Techniques to analyze free-falling strands) of the Deliverable 6.3 “Report on the elaborated engines and software for blending technologies”.

By knowing the distance of the strand from the camera it is possible to use the look-up table to extract the corresponding conversion coefficient, using which it is possible to convert the thickness measurement from pixels to millimeters. Such measurement is then aggregated over multiple strands in order to monitor the trend of the strand thickness, and determine when a deviation from the optimal value occurs.

2.2.6.2 Methods to directly measure thickness

Following a different approach, to make a direct measurement of the thickness of the strand, a bypass is needed in the line where all the strands pass, to take some samples out of it to be analyzed. In fact, both in the mattress and the free-falling scenarios, strands are disposed in an almost chaotic way, very often superimposed, and the number of strands to be analyzed at the same time is too high to guarantee precise and reliable measurements. Furthermore, dust forming in the line makes the measurement more difficult to be done.

To overcome some of these problems and improve conditions for a better measurement of the thickness, strand samples can be separated by means of a dedicated conveyor belt, with a proper speed to permit the strand separation. In addition, a Vibratory conveyor might be used to support this operation [29], by feeding the strands into the conveyor belt.

When the single strand is deposed flat on the conveyor belt, its thickness can be evaluated by taking the belt as reference, i.e. the point with height equal to zero, and measuring the relative height of the strand. To this purpose, laser profilometers can be employed. Figure 11 illustrates this measuring scheme while Figure 12 presents an example of the type of device employed (the Sick Ruler E series [30]). The typical height resolution declared is 0.05 mm, which makes it suitable for measuring the thickness of a strand. Moreover, this device is designed to operate in tough environments, and remotely over long distances using a Gigabit interface.

This solution can be used to evaluate the thickness distribution along the time, allowing to control the strand production in the factory. As a second end, the profilometer might be used to validate the measurement of the thickness estimated from digital cameras images.

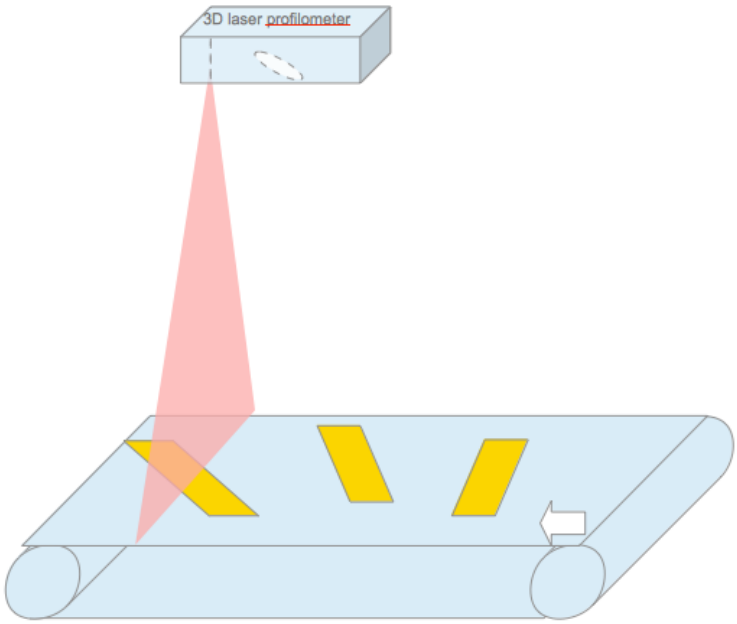

Figure 11 - Estimation of strands' thickness using a 3-D profilometer

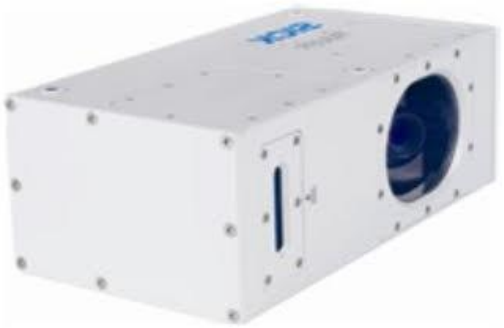

Figure 12 - Example of 3-D profilometer

2.3 EXPERIMENTS

2.3.1 ACQUISITION SETUP

Two Sony XCD-SX90CR color CCD cameras compose the acquisition setup, with a trigger mechanism used to synchronize the two cameras. As shown in Figure 4, the two cameras are arranged horizontally, with an an angle $\alpha = 85°$ with respect to their support. The baseline distance between the cameras is $\Delta_D = 125\ mm$, while the two led bars are place with a vertical orientation at the sides of the cameras, with distances $\Delta_L = 150\ mm$ and $\Delta_S = 100\ mm$. The led bars are chosen and placed in order to have a uniform illumination across the acquisition volume. Moreover, they produce a sufficient light to be able to capture the falling strands using a low shutter, and avoid possible motion blur effects.

2.3.2 ACQUISITION PROCEDURE

The acquisition procedure consists in making the strands fall in front of the cameras. The behaviour of the strands falling in front of the cameras with high frame rate was studied, and then it was observed that high variations in the falling phenomenon are present, regarding the speed, orientation and position of the strands at the moment of the image acquisition. Moreover, the height from which the strands fall is not always constant. For these reason, the processing system for performing the granulometric analysis of the falling strands was studied in order to be robust to these variations, which are intrinsic in the falling phenomenon.

However, the falling speed and height cannot be controlled, as well as the speed, position, and orientation of the strands at the time of the acquisition. Then, an accurate description of these parameters is not reported. Moreover, in some cases the acquisitions are not usable, due to obstructions or particular orientations of the strands, and so the proposed system performs a sample analysis of the strands, by using only the images where the strands are visible.

2.3.3 ROBUSTNESS TO ENVIRONMENTAL CONDITIONS

The experiments were performed using strands with different colors, different positions of the lights, and considering both daylight and artificial illumination, with the result that the method is not significantly affected by variations of this factors.

2.3.4 WORKING RANGE

In order to estimate the working range of the proposed method, first we estimated the lower limit of the system by considering a set of spheres with diameters ranging from 3 to $11\ mm$. We captured the spheres

using the acquisition procedure described in Section 2.3.2, and observed that only the spheres with a diameter of at least $4\ mm$ were detected correctly.

Moreover, a similar analysis was performed by capturing a set of strands smaller than the average strand size, in particular with length varying from 13 to $29\ mm$, and with width varying from 2 to $7\ mm$. In agreement with the result obtained by measuring the spheres, only the strands that have a width > 4 mm were correctly detected. However, the surface of the strand must be visible in the cameras in order to be correctly detected.

Then, we estimated the upper limit of the working range as equal to the acquisition volume, which is equal to $W\ x\ H\ x\ D = 400\ x\ 225\ x\ 500\ mm$ in the considered acquisition setup.

2.3.5 ACCURACY OF GRANULOMETRIC ANALYSIS

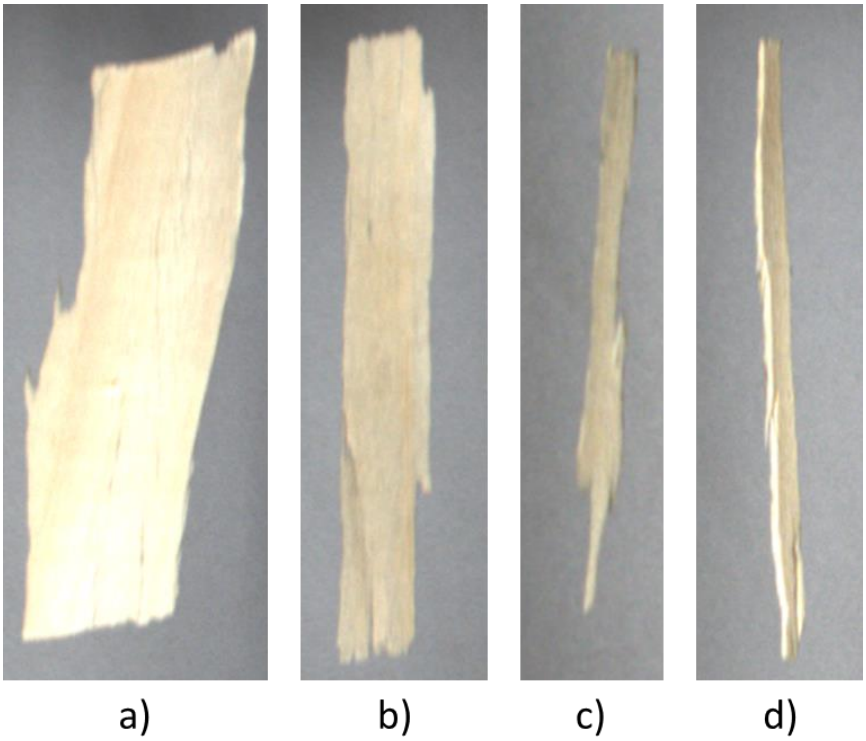

Figure 13 - Examples of strands captured with the Camera A: (a,b) strands compliant to the reference size provided by the manufacturing industry; (c,d) strands non-compliant to the reference size. The strands in (c,d) have a lower width with respect to the strand

The accuracy of the proposed approach was tested by considering a databased composed by two types of strands, which represent the different working conditions in a real industry: the first type of strands is compliant with the reference size provided by the manufacturing industry, and feature an average size equal to $L\ x\ W = 116\ \mathrm{x}\ 22\ \mathrm{mm}$ (Figure 13a,b). We collected 50 strands of the first type, and captured each strand 20 times.

The second type of strands does not comply with the reference size, and have an average size equal to $L\ x\ W = 91\ \mathrm{x}\ 10\ \mathrm{mm}$ (Figure 13c,d). This type of strands can be caused by stranding errors, wearing of the tools or the transport systems, etc. We collected 50 strands of this type, and captured each strand 20 times.

The total number of two-view acquisitions is then $50\ x\ 20\ =\ 1000$. The sizes of the strands have then been organized into bins, and the percentage of strands for each bin is shown in Table 1.

The real sizes of the strands were computed by using calipers to perform the measurement, according to the standard measurement procedure [31]. However, since the strand shape is not regular, the measurement have an uncertainty of about 3 mm, depending on how the procedure is interpreted.

		Width				
		0-10	**11-20**	**21-30**	**31-40**	**41-50**
Length	**30-60**	0	2	1	0	0
	61-90	11	8	2	0	0
	91-120	13	17	26	6	0
	121-150	4	3	4	2	1

Table 1 - Real strand sizes, classified into bins (%)

The proposed method was applied on all the captured strands, of both typologies. In particular, for each strand we considered the average size computed by considering the 20 acquisitions. The distribution of the strands into each bin, according to the measured sizes, is shown in Table 2 as percentages of the total number of strands. Based on this results, it was possible to observe that the width of the strands influences more the accuracy of the measurement, more than their length.

		Width				
		0-10	**11-20**	**21-30**	**31-40**	**41-50**
Length	**30-60**	2	5	1	0	0
	61-90	9	6	1	0	0
	91-120	12	19	20	1	0
	121-150	4	9	9	2	0

Table 2 - Computed strand sizes, classified into bins (%)

Then, as a second figure of merit, we aggregated the classification error according to the width of the strands. The results are shown in Table 3. In particular, the error is computed according to each width bin, using the results shown in Table 1 and Table 2, using the formula:

$$c_j = \frac{|\sum_{i=1}^{N_b} T_r(i,j) - \sum_{i=1}^{N_b} T_c(i,j)|}{N_s} \quad \forall j$$

Where c_j is the classification error for the width bin j, i is the i-th length bin, N_b is the number of length bins, T_r and T_c represent the tables with the real and computed strand distributions (Table 1 and Table 2, respectively), N_s is the total number of strands.

Width

	0-10	11-20	21-30	31-40	41-50
Classification error (%)	1	9	2	5	1

Table 3 - Classification error according to the strand width

By observing the values reported in Table 3, it is possible to notice that the classification error is always $< 10\%$, with the consequence that it is possible to use the method for the granulometric analysis of falling strands. Moreover, the method can be used for determining when the measured strands no longer feature a size compliant with the reference size.

3 ANALYSIS OF THE STRANDS AFTER THE BLENDING PROCESS

This section describes the techniques used for analyzing the strands after going through the blending process. In particular, a hardware acquisition setup and two image processing algorithms have been designed and implemented in order to estimate the size distribution of the strands after they have been laid on the conveyor belt.

3.1 LAYOUT OF THE VISION-BASED SYSTEM

This section describes the layout of the vision system of the prototype proposed by UMIL to monitor the mat-forming process.

According to the physical constraints that appear in the production plant, two different acquisition setups have been projected. The main differences in their deployment is the placement of the illumination elements. Hereafter, they will be called acquisition setup A and B. Acquisition setups A is preferred to acquisition setup B. Hence, if possible, acquisition setup A should be the one installed.

Figure 14 and Figure 15 show the layout of Acquisition setup A from a side and top view, respectively.

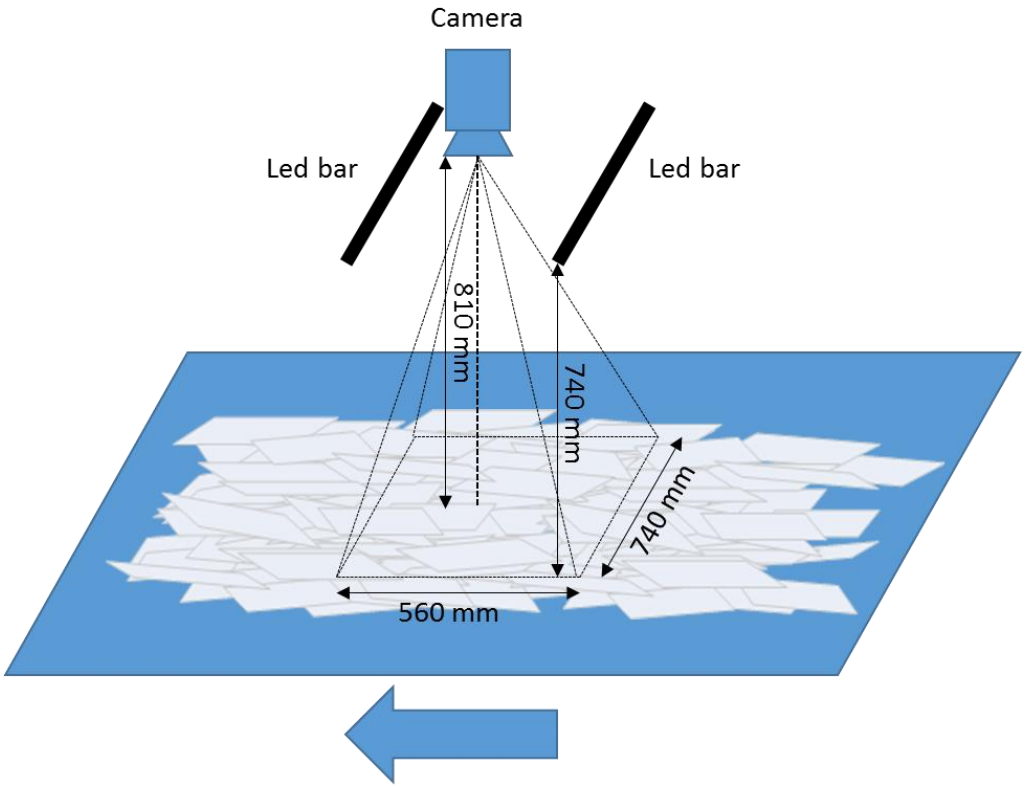

Figure 14 - Layout of the acquisition system A (side view). The arrow represent the direction in which the mattress moves.

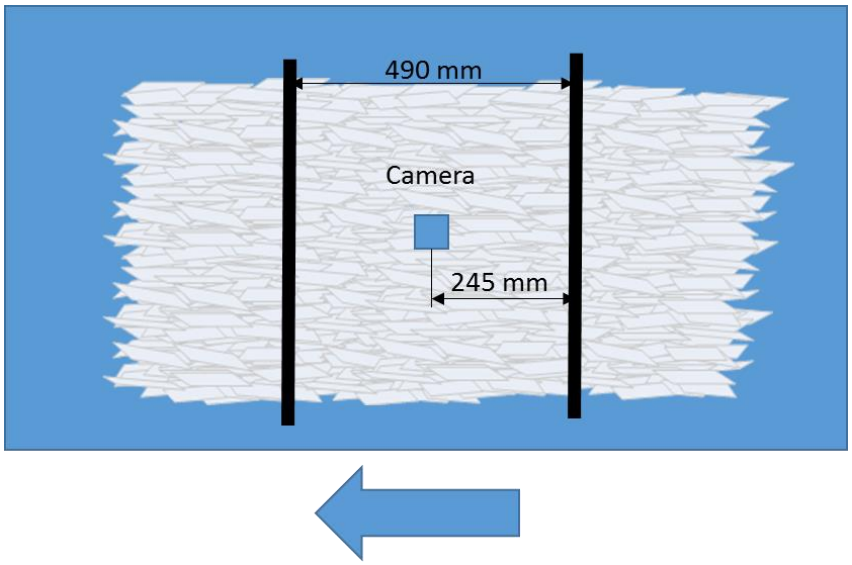

Figure 15 - Layout of the acquisition system A (top view). The arrow represent the direction in which the mattress moves.

In case it is impossible to deploy acquisition setup A, due to physical constraints, acquisition setup B has been designed. The main difference with the previous setup is the disposition of the illumination elements, which are placed parallel to the movement of the conveyor belt. Figure 16 and Figure 17 illustrate the structure of acquisition setup B from the side and top view, respectively.

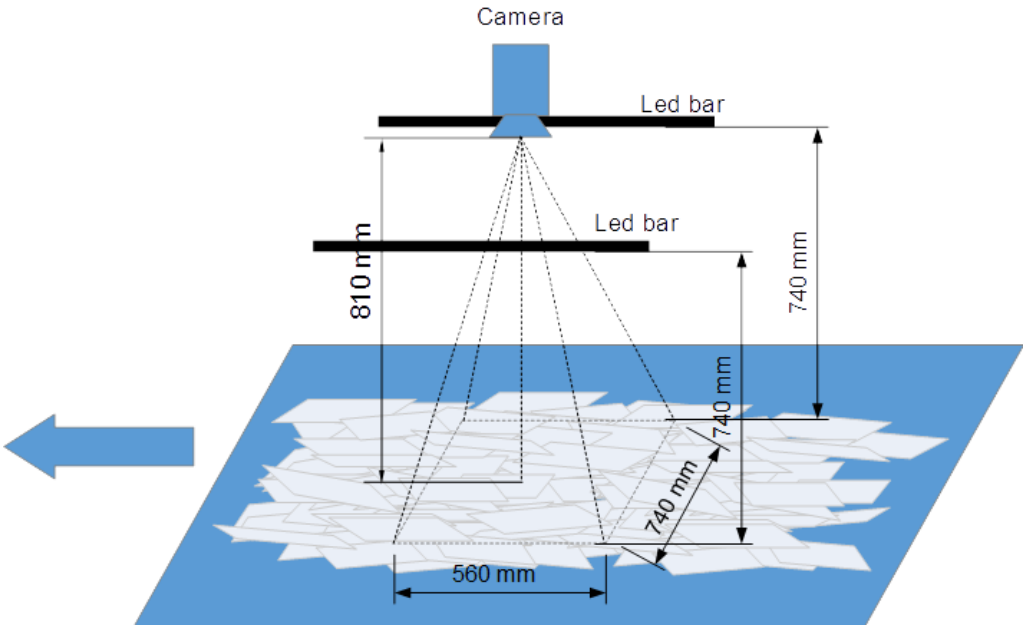

Figure 16 – Layout of the acquisition system B (side view). The arrow represent the direction in which the mattress moves.

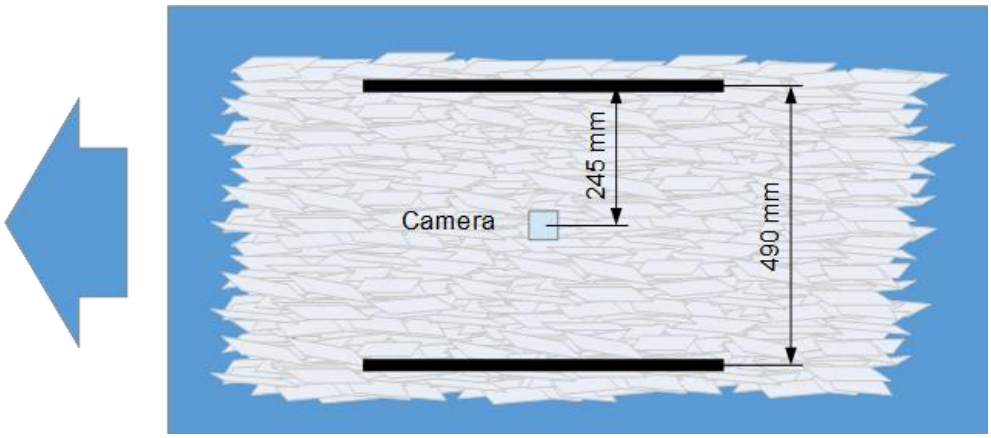

Figure 17 – Layout of the acquisition system B (top view). The arrow represent the direction in which the mattress moves.

3.2 GRANULOMETRY ANALYSIS BASED ON SEGMENTATION

The estimation of particle size distributions of the strands disposed on the conveyor belt poses some important image processing challenges:

- The strand's characteristic shape, rectangular with a side much longer than the other, generates many occlusions, which, in many cases, divide the strands into pieces, making more difficult size estimation.
- The strand's colors are very similar in the majority of cases. Hence, it is difficult to differentiate them using traditional techniques.

This section introduces a framework that has been particularly tailored to face these problems. This framework is capable of estimating the granulometry of wood strands particles laid on a conveyor belt. The proposal has a threefold novelty:

1. It is the first approach that, using two-dimensional computer vision analysis, permits to study the granulometry of huge amounts of wood strands that have been randomly placed on a conveyor belt. The approaches that can be found in literature perform an offline analysis of small amounts of material. In addition, they require that the particles are not superimposed. Other approaches employ complex and expensive devices, like 3D-profilometers [29].
2. The methods employed, which include innovative clustering and post-processing methods, have been designed to be better adapted to the specific characteristics of the application problem.
3. The tests performed to analyze the performance use two different kinds of images:
   a. Real images of wood strands that permit the study of the performance in a real setup
   b. Synthetic images that allow the analysis of the robustness and accuracy of the approach with regard to small variations in the materials

The designed process is divided into two phases: particle identification and size estimation. Particle identification is the most challenging phase with respect to image processing. This phase is performed employing optimized fuzzy color clustering. This method is able to locate the objects with the lightest colors present in the image. These particles will reasonably correspond to the strands laid on the mattress' surface. In addition, these strands usually present less occlusions, because they are not behind superimposed strands. Furthermore, to facilitate the location of small strands, while maximizing the number of located strands, the method is applied block-wise, following a pyramidal structure. Figure 18 shows the blocks employed in the process. In order to detect strands that may be located at the borders of

the blocks, the different blocks are overlapped. In addition, the different sizes of the blocks make the algorithm capable of detecting both small and big strands.

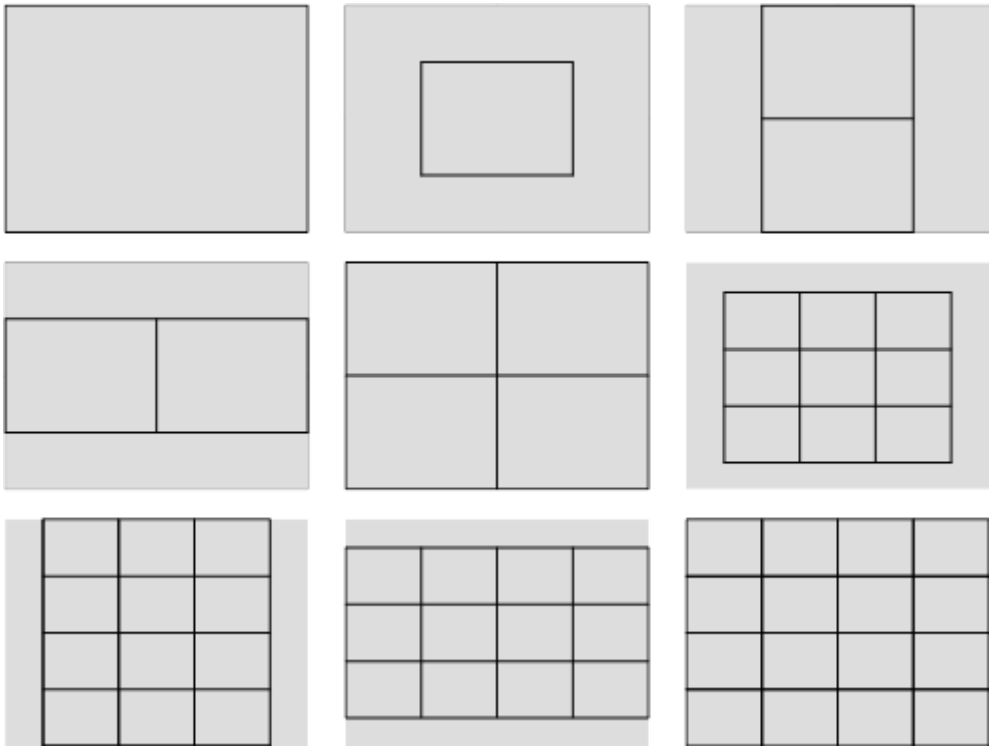

Figure 18 - Blocks used to perform the segmentation.

The particle identification process is performed in three steps, which are independently applied for each block (see Figure 19): image enhancement, particle segmentation and particle selection.

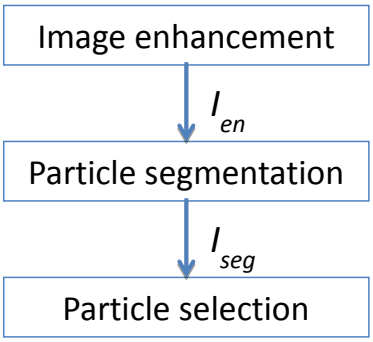

Figure 19 - Particle identification steps.

3.2.1 IMAGE ENHANCEMENT

The image enhancement step applies the following operations:

- The edges in the image *I* are highlighted using a Laplacian filter. This step is crucial since the edges are play an important role in the separation of the strands. Formally: $I_{en} = I + k[\nabla^2(I)]$, where $\nabla^2(I)$ represents the Laplacian of *I*, and *k=1* or *k=-1* according to the derivative definition.
- In order to enhance contrast, a histogram equalization.
- The edges in *I* are detected using Canny algorithm [32]. Successively they are dilated using a circular kernel of one pixel of radius, and subtracted from *I* to produce I_{en}. Using this approach it is possible to help the algorithm to differentiate the strands that have similar colors and are close to each other.

3.2.2 PARTICLE SEGMENTATION

In order to isolate the particles that have lightest colors, Fuzzy C-Means (FCM) clustering algorithm [33] is used. In particular, all the pixels in image I_{en} are clustered according to their RGB channels. In contrast to traditional clustering algorithms, the partition produced using FCM provides a degree of membership between [0,1], permitting each pixel to belong to more than one cluster.

To produce the partition, FCM minimizes the following objective function:

$$F_m = \sum_{i=1}^{n}\sum_{c=1}^{C} u_{ic}^{m} \parallel \mathbf{x}_i - \mathbf{v}_c \parallel^2,$$

where m represents the "fuzziness" of the clustering, n indicates the number of pixels in the image, U_{ic} is the degree of membership of pixel x_i to the c-th cluster, v_c is the center of the c-th cluster.

FCM produces the following outputs:

- C cluster prototypes, which are represented by the vectors v_c, for c=1,…,C.
- a fuzzy partition matrix $\mathbf{U} = [u_{ic}]_{i=1\ldots n}^{c=1\ldots C}$, in which U_{ic} indicates the degree of membership of pixel x_i to cluster number c.

For the problem of strand segmentation, the number of clusters was experimentally selected to be three. From these three clusters, the one with the lightest color is chosen. As output of the clustering, an image representing the degree of membership of each pixel to the chosen cluster is obtained. After that, the image is transformed binarized using Otsu's method [34], obtaining a binary image I_{seg}.

3.2.3 PARTICLE SELECTION

Once I_{seg} has been obtained, the particles that appear on it are selected by applying different filters to the connected components α. The parameters used by these filters were experimentally determined.

As a result, the image I_p is obtained:

$$I_p = I_{seg} - \bigcup_{\alpha \in I_{seg} | cond} \alpha,$$

where *cond* is a set of morphological conditions that helps to clean the image from particles that do not represent strands. In particular, three different conditions are checked:

- To discard those connected components that do not represent strands, and consequently can be considered as noise, all the components with area $A(\alpha)$ smaller than the 30% of the area of the biggest component, denoted as a_{max}, are eliminated. Formally, $cond_1 : A(\alpha) < 0.3\ a_{max}$.
- In most cases, strands are much longer than wider. Hence, those components whose relation between major axis, $M(\alpha)$, and minor axis, $m(\alpha)$, is less than a specified value, r_1 =2, are ignored. Formally, $cond_2$: $M(\alpha)/\ m(\alpha) < r_1$.
- Likewise, as the majority of the strands have a shape that approximates that of a rectangle, those components whose area or perimeter are much larger or smaller than the area or perimeter of an ideal rectangle of similar dimensions are rejected. In particular, if the relation between ideal area/actual area or the relation between ideal perimeter/actual perimeter are higher than r_2=0.5, the component is discarded. Formally: $cond_3$: $(2M(\alpha) + 2m(\alpha))/p(\alpha) > r_2$ or $M(\alpha)\ m(\alpha)\ /a(\alpha) > r_2$, where a(α) and p(α) stand for area and perimeter, respectively.

The particles obtained after these step are the base from which granulometry is estimated. Figure 20 illustrates the whole process followed to obtain the particle size distribution of an image.

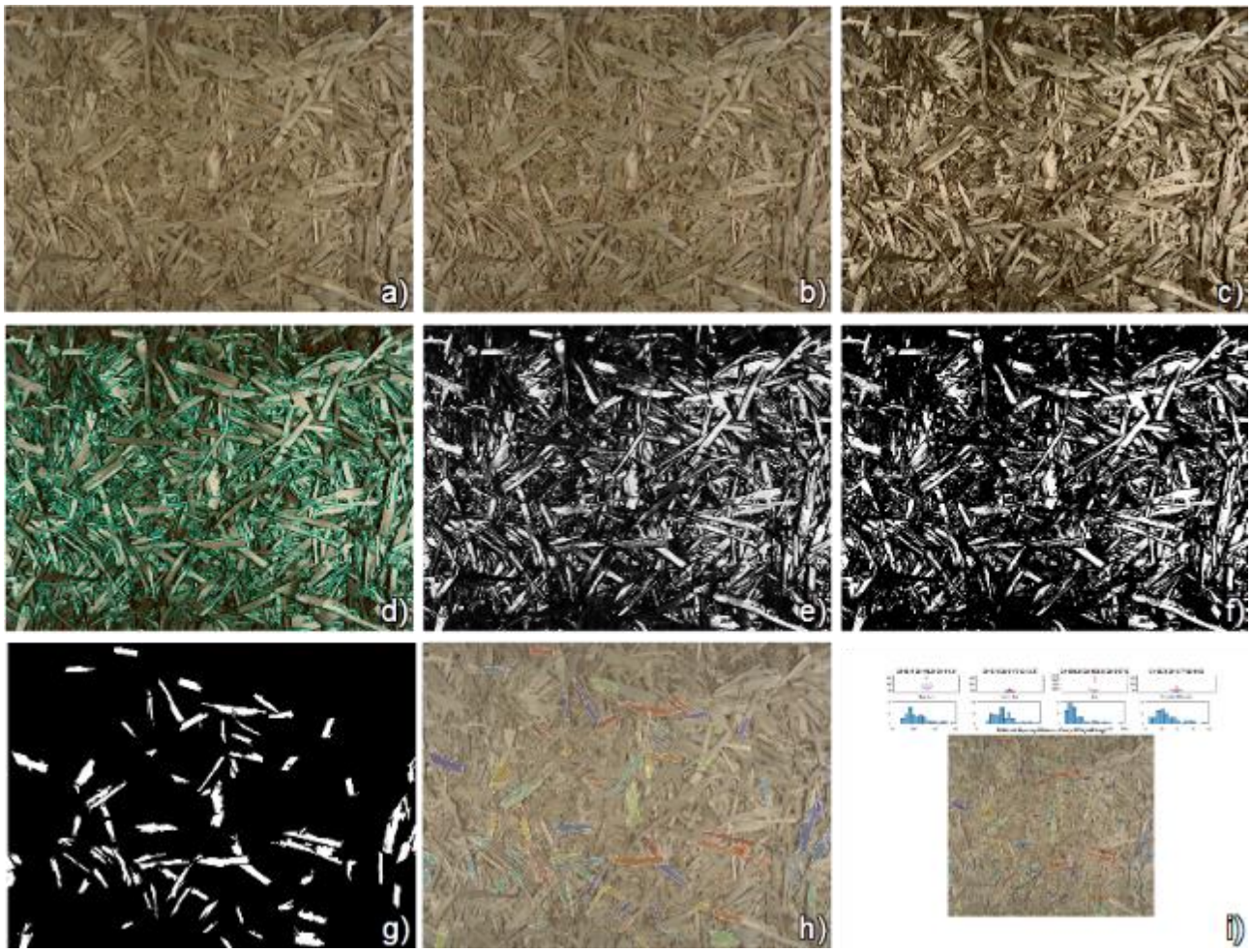

Figure 20 - Examples of the different steps followed to obtain the final granulometry. a) the initial image. b) result of the Laplacian filter. c) result of the contrast enhancement. d) result of the edge elimination. e) result after clustering. f) result after binarization. g) final segmentation. h) segmenation superimposed on the original image. i) analysis of the granulometry, which presents boxplots and histograms for four measurements: major axis, minor axis, equivalent diameter and area.

3.3 QUALITY ANALYSIS IN FREQUENCY DOMAIN

In contrast with most common approaches, and with the previous approach, the method presented in this section does not perform measurements of every particle by using segmentation algorithms. This approach has the potential to obtain accurate quantitative results, but requires a controlled environment to obtain satisfactory results, and is computationally expensive.

In some cases, where the environmental conditions are less favorable, it can be more useful to use a robust qualitative approach. This qualitative analysis takes into account the target strand quality defined in the DoW.

This section introduces an approach that avoids segmentation and is capable of obtaining a robust behavior by analyzing the frequency domain. This approach can be particularly useful in the industrial scenario considered in this document. In particular, in an industrial setup it is possible to find changes in the environmental conditions that may affect the vision based systems, like:

- Changes in illumination that can change color and gray-tone distributions;
- Presence of dust particles that can reduce the visibility of the camera, making more difficult the process of particle measuring.;

- Changes in the materials employed in the production, for example, different woods may produce particles with different colors.

The presented approach, which analyses the frequency domain, has the following advantages:

- It is flexible against changes in the environment, for instance, illumination conditions, presence of dust…;
- It is very robust, and hence, can be used online;
- It is capable of identifying, during manufacturing, situations in which the quality of the produced strands has significantly changed. In this sense, it can emulate the capabilities of an expert operator, and detect deviations from the optimal operating point specified for the factory.

This approach presents a two-fold novelty:

1. It avoids segmentation, making the method more robust against environmental variations.
2. It is the first approach that analyzes Fourier transform to provide quality estimations of wood particles in an industrial setup. The majority of the approaches presented in the past are segmentation-based. On the other hand, those methods that analyze the frequency domain perform only preliminary studies, and have not been applied to online analysis.

3.3.1 DESCRIPTION OF THE METHOD

As indicated in Section 3.2, the estimation of the size of wood particles using segmentation is difficult because:

- the strand's characteristic shape, rectangular with a side much longer than the other, generates many occlusions, which, in many cases, divide the strands into pieces, making more difficult size estimation.
- the strand's colors are very similar in the majority of cases. Hence, it is difficult to differentiate them using traditional techniques.

To deal with these problems, the proposed approach estimates quality analyzing the frequency domain. In particular, the method quantizes the Fourier transform in order to obtain a histogram that summarizes the information contained on it. Later, the histogram is used to classify wood strands' quality by means of a k-NN classifier.

The 2-D Discrete Fourier Transform of an image can be defined as [35]:

$$F(u,v) = \sum_{x=0}^{M-1} \sum_{y=0}^{N-1} f(x,y) e^{-j2\pi(\frac{ux}{M} + \frac{vy}{N})}$$

for frequencies u= 0, 1,…, M-1 and v= 0, 1,…, N-1. Where the function $f(x,y)$ represents an image of size M × N. $F(u,v)$ is, generally, a complex function that can be analyzed both in terms of magnitude and phase. Let us denote the real and imaginary part of $F(u,v)$ as $R(u,v)$ and $I(u,v)$, respectively. The proposed system examines the power spectrum, defined as:

$$P(u,v) = R^2(u,v) + I^2(u,v)$$

The approach partitions $P(u,v)$ into radial bands of one pixel of width. Where each band is formally defined as:

$$B(r) = \{(u,v) : r = \left\lfloor \sqrt{(u-u_c)^2 + (v-v_c)^2} \right\rfloor\}$$

for $r = 1, \cdots, \left\lfloor \sqrt{\frac{M}{2}^2 + \frac{N}{2}^2} \right\rfloor$, where u_c and v_c are the coordinates of the center of the Fourier transform. Figure 21 illustrates the partitions used to produce the histogram.

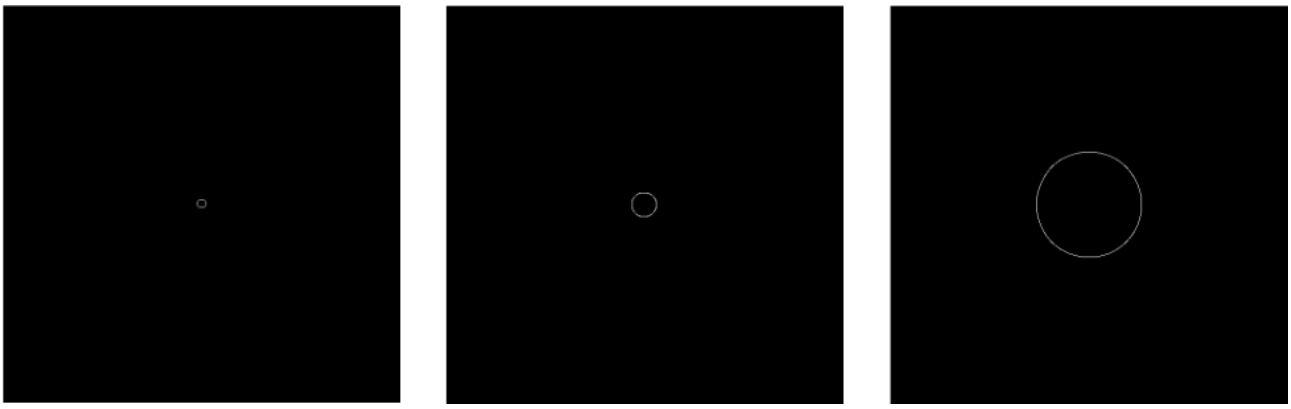

Figure 21 - Examples of the bands used to produce the histogram

For each band the histogram is defined as:

$$H(r) = \sum_{(u,v)\in B(r)} P(u,v)$$

Where, *H(r)* summarizes the energy present in frequency *r,* both in horizontal and vertical direction. With the bands near the center summarizing the power in low frequencies and those far from the center the power from high frequencies.

The final output is a histogram that represents the energy, Figure 22 shows the process of histogram calculation for an image containing real wood strands, including the image, its Fourier transform and the final histogram. While Figure 23 compares the histograms obtained from images that contain strands of different quality.

To classify the quality of the wood strands present in the image, these histograms are exploited using a computational intelligence classification model. Particularly, the chosen model has been k-Nearest Neighbors (k-NN) [36]. k-NN does not calculate an explicit classification model, in contrast, it stores the learning instances and compares the new instance with them, indicating the class of the instance that is most similar to the new one. This kind of classification technique is called instance-based machine learning algorithm.

The model is learned following this process:

- for each image *j* in the training database, histogram H_j is calculated.
- successively, every H_j needs to be normalized, obtaining $\widehat{H_J}$, so that $\widehat{H_J} \in [0,1]$ for $r = 1, \cdots, \left\lfloor \sqrt{\frac{M}{2}^2 + \frac{N}{2}^2} \right\rfloor$.
- to represent the model, each $\widehat{H_J}$ is stored.

The following method is applied in order to classify a new instance *x*:

- the histogram is extracted and normalized. To perform the normalization, the values used in the learning process are employed.
- The Euclidean distance d_{jx} is calculated between each histogram $\widehat{H_j}$ and the new instance *x*.
- The *k* members of the training set that have the minimum distance d_{jx} to instance *x* are grouped in set *K.*
- The final classification result is chosen as the most frequent class in *K.* If a tie appears, it is broken using d_{jx}.

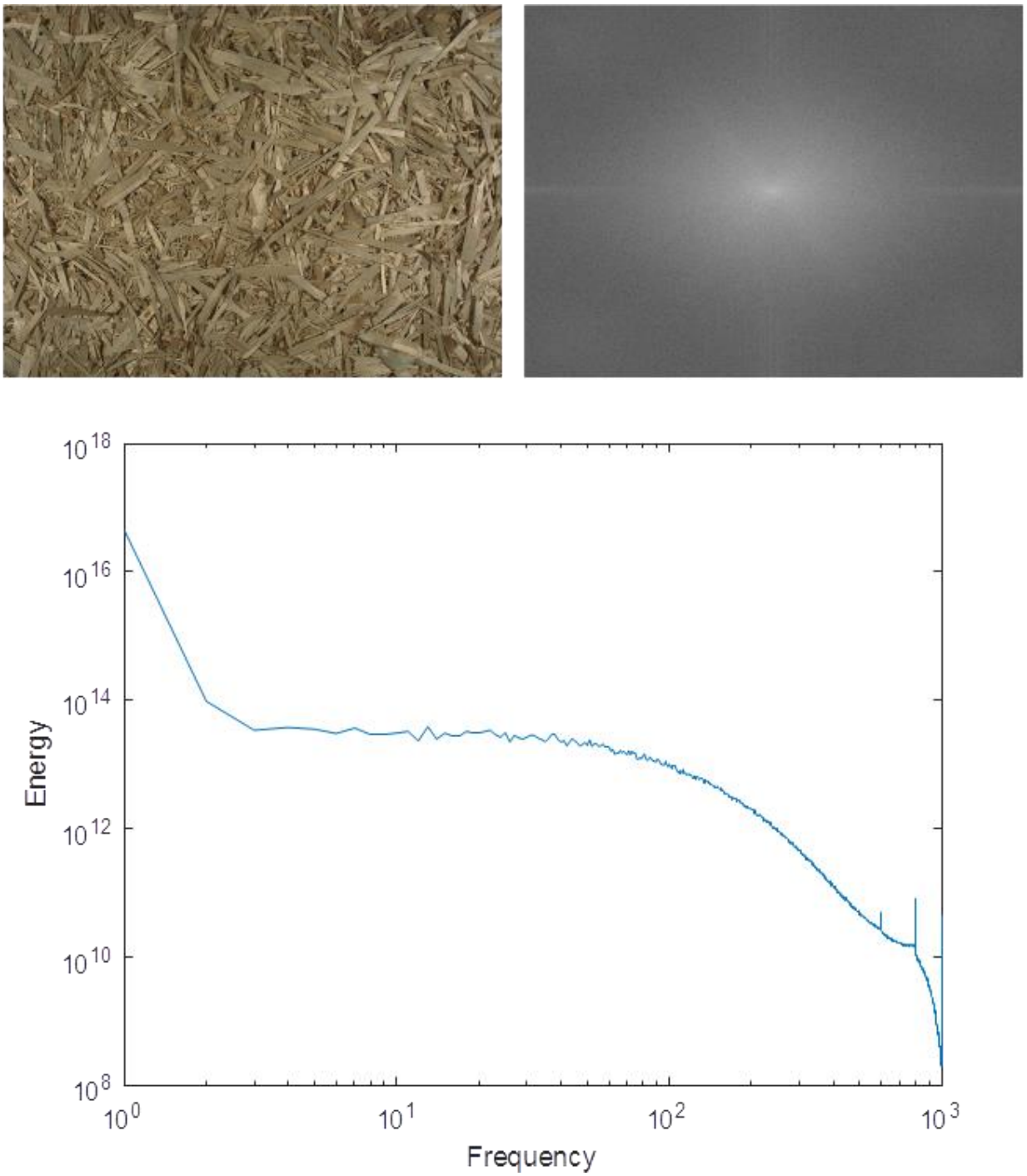

Figure 22 - Histogram extracted from an image with resolution 1200 × 1600, which presents including real strands of low quality. Top-left, original image. Top-right, magnitude of the Fourier transform. Bottom, the final histogram displayed as a log-log plot.

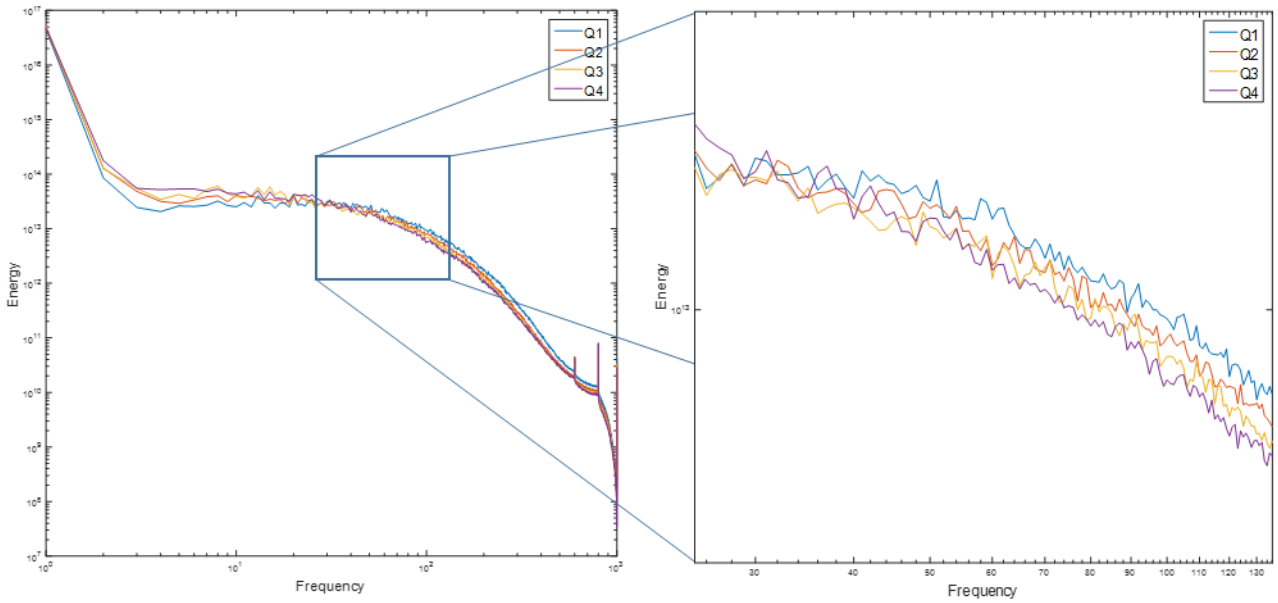

Figure 23 - Comparison of histograms obtained from images with strands of diverse qualities.

3.4 A METHOD TO GENERATE REALISTIC SYNTHETIC IMAGES

This section introduces a method capable of generating realistic synthetic images of wood strands laid to form a mattress. The produced images are used in Section 3.5 to test the methods that have been introduced in this deliverable. The main advantage of using synthetic images is that it is possible to control the parameters of the strands and the environmental conditions. In this way, the tests can be very exhaustive and the results can be rigorously analyzed. In particular, some of the aspects that can be directly controlled by the proposed method are:

- The size of the strands, and its distribution if it is necessary to simulate wood strands of different sizes.
- The angle in which the strands are laid and its distribution if it is necessary to simulate varying angles.
- The chromatic palette. Which permits the simulation of different ambient lights and non-uniform lighting.

The method randomly distributes wood strands, simulated as rectangles, on a 3-D environment. After that, to provide a more realistic result, the image is enriched with simulated shadows. The method is divided in the following steps:

1. Acquisition of the chromatic palette. In this step, the colors of the wood strands are generated. In general, and to make the results more realistic, this process is performed by randomly acquiring the colors from a real image.
2. Laying of the simulated wood strands. This step distributes the strands in the artificial mattress. The process is performed on a layer basis. Starting from the bottom of the mattress, each layer is populated by a predefined number of strands, until the top of the mattress is reached. For each strand, the following steps are followed:
    a. The length and width of the strand is generated using the parameters specified at the beginning of the process, which specify their limits and distributions.
    b. The height of the mattress at which the strand is laid, position in the Z-axis, is chosen according to the layer being completed.
    c. The position in the X-axis and Y-axis are randomly generated, avoiding the superposition of strands in the same layer.
    d. The angles of pitch, roll and yaw are generated according to the parameters introduced, which include their limits and distributions.

e. The color of the strand is randomly selected from the chromatic palette. In general, the strands located in the lowest layers have darker colors, and those located in the highest layers, have lighter colors.

3. Shadow casting. This step simulates the shadows of the strands, to create a more realistic result.

Figure 24 illustrates the type of mattress generated using the proposed method. In particular, the mattress can be seen from different angles and after the shadows have been simulated.

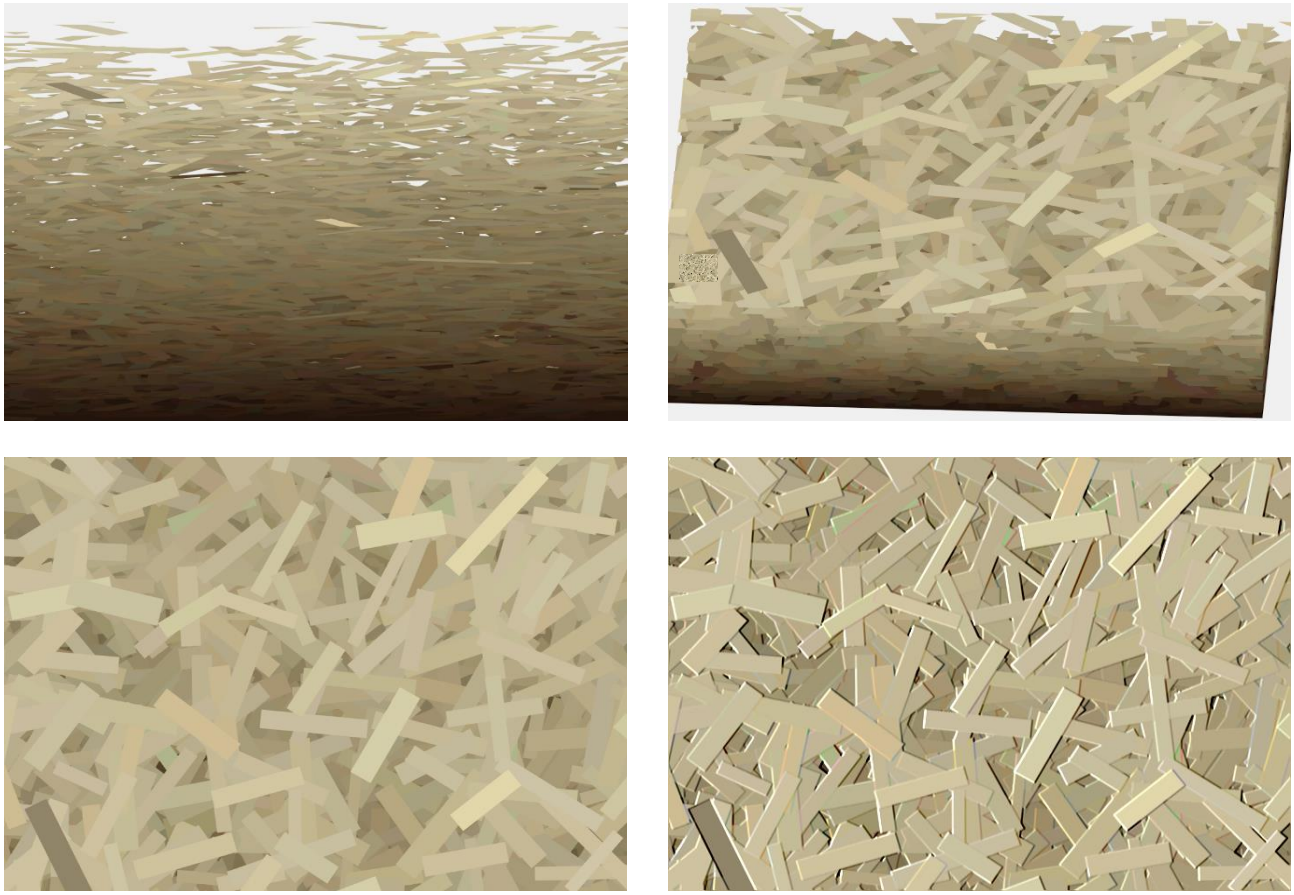

Figure 24 - A synthetic mattress from different angles.

3.5 EXPERIMENTS

This section analyzes the performance of the proposed methods to evaluate the size and quality of the strands.

3.5.1 ANALYSIS OF THE SEGMENTATION-BASED METHOD

In this section, the results obtained by the segmentation-based approach are analyzed, using both real and artificial images. The employed images have a resolution of 1600×1200 pixels. Figure 25 shows examples of these images.

3.5.1.1 Tests using real images

This section studies the performance of the proposed approach for images captured from a real mattress. Table 4 summarizes the results obtained for images that include: mainly big strands, mainly small strands, strands with a mixture of sizes. The results show the average first, second and third quartiles (Q1, Q2, and Q3) obtained for each type of image. For each image type, the test database included 10 images. In addition, Figure 26 shows examples of the histograms that summarize size distributions, obtained for three different test images. In order to analyze the ability of the proposed approach to discriminate between

different strand distributions, Student's t-test was applied to the results. In particular, a statistical study that compares in a

Figure 25 - Examples of the images used in the tests. First column shows images of the real mattress, second column presents synthetic images. The size of the strands present in the images increases from top to bottom.

pairwise way the quartiles obtained in the experiments can indicate if the results obtained are precise enough to distinguish images that contain strands of different sizes. The results of the statistical tests indicate that the differences in the results are significant with α=0.02 for all cases except one. The exception is the comparison of Q2 in the images containing only small strands and a mixture of small and big strands. These results indicate that the proposed approach can detect significant changes in the granulometry of the wood strands. This is particularly important, since in this way the proposed algorithm

can emulate the results obtained by an expert operator. Thus, the approach fulfills the requirements that motivated its development.

	MINOR AXIS				MAJOR AXIS		
	Q1	Q2	Q3		Q1	Q2	Q3
BIG	13.2	16.9	21.7		46.4	61.2	87.5
MIX	9.6	12.5	16.7		40.1	52.0	74.9
SMALL	8.5	10.9	14.3		37.7	49.6	68.0

Table 4 - Results, in mm, obtained using mattress images.

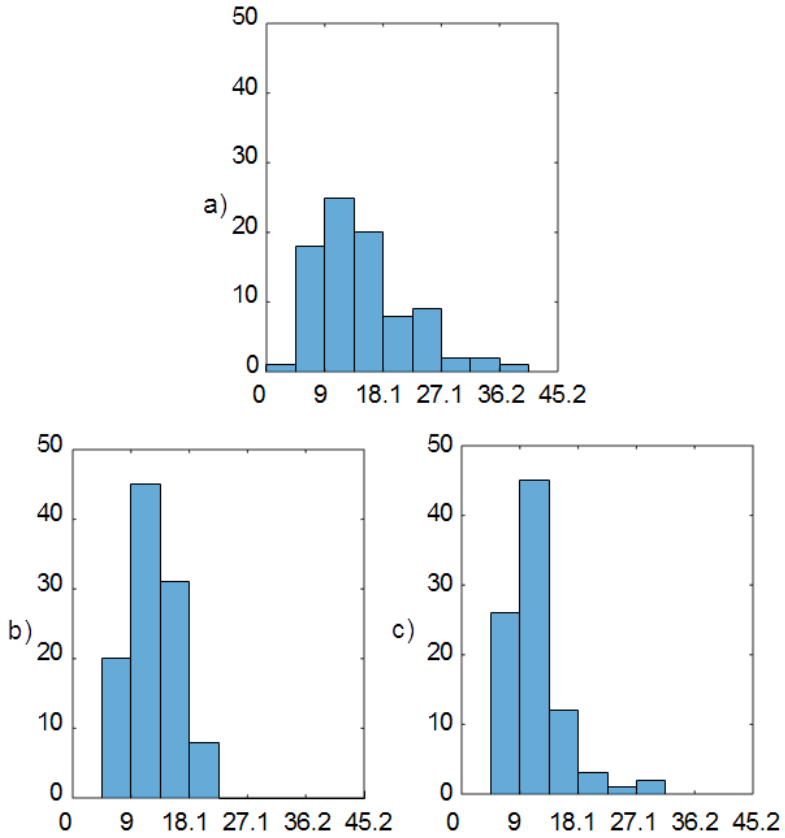

Figure 26 - Histograms obtained for the minor axis of real images: a) image containing only big strands, b) image containing both small and big strands, c) image containing only small strands. The results show how, as the proportion of small strands present in the image grows, the approach detects less strands with a big minor axis and more with a small minor axis.

3.5.1.2 Tests using synthetic images

This section studies the performance of the proposed approach for synthetic images. As illustrated in Section 3.4, the generation of synthetic images permits to maintain determined parameters under control, specifying with high precision their values. For instance, regulating the sizes of the major and minor axis, or the chromatic palettes. In this way, it is possible to estimate precisely the accuracy and robustness of the proposed approach. This study is very complex when real images are used. Figure 25 shows examples of the types of images used to perform these tests.

In particular, three different simulated setups have been employed in these tests. Each one of these setups uses a different normal distribution to determine the sizes of the strands. Respectively, the parameters of the three setups are μ= {20, 17.5, 15} and σ= {4, 5, 6} for the minor axis and μ= {100, 80, 60} and σ= {20, 30, 40} for the major axis. The experiments included 100 images for each setup.

Table 5 presents the obtained average results. This table includes the real values used in the generation of the synthetic images and those estimated by the proposed method. These results illustrate the ability of the proposed approach to detect changes with a satisfactory accuracy (an average error of 6.8%).

To assess if the method can effectively detect significant differences in strand distributions, a statistical test, similar to the one used in Section 3.5.1.1, was used. The results of the test indicate that there are significant differences for all cases with α=0.01.

		MINOR AXIS				MAJOR AXIS		
		Q1	Q2	Q3		Q1	Q2	Q3
SETUP 1	Real dimensions	17.3	20.0	22.7		86.6	100.1	113.6
	Obtained granulometry	16.8	20.7	24.6		66.8	94.2	119.8
SETUP 2	Real dimensions	14.1	17.5	20.9		64.8	82.9	102.1
	Obtained granulometry	14.3	18.4	22.9		58.4	79.4	105.1
SETUP 3	Real dimensions	10.4	14.6	18.8		50.9	71.0	94.2
	Obtained granulometry	12.1	16.4	21.3		52.0	71.7	97.5

Table 5 - Results in mm obtained using artificial images.

3.5.2 ANALYSIS OF THE FREQUENCY-BASED METHOD

This section studies the performance of the approach based on the analysis of the frequency transform of the image. The study is performed using 40 images acquired using the setup introduced in Section 3.1. To test the robustness of the proposed approach, the test also analyzes its performance when different types of noise are added to the images. Figure 27 shows some of the original images used in the test of this section. For each experiment, the accuracy of the proposed approach is estimated using 10-fold cross validation.

3.5.2.1 Accuracy analysis on a real scenario

This section studies the results obtained for the ideal setup, in which there is not noise. The experiments consider four different quality classes, C_1,..., C_4. Each quality class contains a different proportion of low and high quality wood strands. In particular, the approximate proportion of high quality strands is {0, 0.3, 0.6, 1} beginning from C_1. For each quality class C_i, the database contained 10 images.

Two different experiments were performed, each one using a different resolution. The first experiment used images with resolution 1600×1200 pixels. The second experiment employed images with resolution 800×600 pixels. This study permits to analyze if it is possible to reduce the cost of the quality estimation, in both computational time and acquisition hardware, without reducing the performance.

Table 6 shows the confusion matrixes obtained in the experiments. Two setups were used for each experiment, one using 1-NN and the other using 3-NN. The results obtained for the first experiment, using the highest resolution, are very satisfactory. An average accuracy of 96% and 98% were obtained using 1-NN and 3-NN, respectively. For the second experiment, there is a slight accuracy drop, caused by the reduction in resolution. However, the results are still very satisfactory, with an average accuracy of 94% and

96% using 1-NN and 3-NN, respectively. A more detailed analysis of the confusion matrixes indicates that, independently of image resolution, the proposed approach can effectively detect significant changes in the quality of the wood strands.

Figure 27 Examples of the images of real wood particles used in the tests. The quality of the strands, according to the target specifications indicated for the project, increases from left to right and from top to bottom.

	1600×1200 PIXELS									800×600 PIXELS								
	1-NN					3-NN				1-NN					3-NN			
	C_1	C_2	C_3	C_4		C_1	C_2	C_3	C_4	C_1	C_2	C_3	C_4		C_1	C_2	C_3	C_4
$\dot{C}_1$	1	0	0	0		1	0	0	0	1	0	0	0		1	0	0	0
$\dot{C}_2$	0	1	0.2	0		0	1	0.1	0	0	1	0	0		0	1	0.1	0
$\dot{C}_3$	0	0	0.8	0		0	0	0.9	0	0	0	0.8	0.1		0	0	0.8	0
$\dot{C}_4$	0	0	0	1		0	0	0	1	0	0	0.2	0.9		0	0	0.1	1

Table 6 - Mean confusion matrices obtained for real images.

3.5.2.2 Accuracy analysis in noisy environments

This section studies the behavior of the frequency-based approach when the environmental conditions are adverse. In particular, two types of noise have been simulated (Figure 28 illustrates the type of noise and the amount of it present in the test images):

- Device noise, which was simulated using salt and pepper noise at different density values: *d*={0.01, 0.02, 0.04, 0.08}.
- The type of noise caused by a dirty lens or by an out of focus problem, which was simulated using a Gaussian blur generated with different kernel sizes: {2, 4, 8, 16} and standard deviations: {1, 2, 4, 8}.

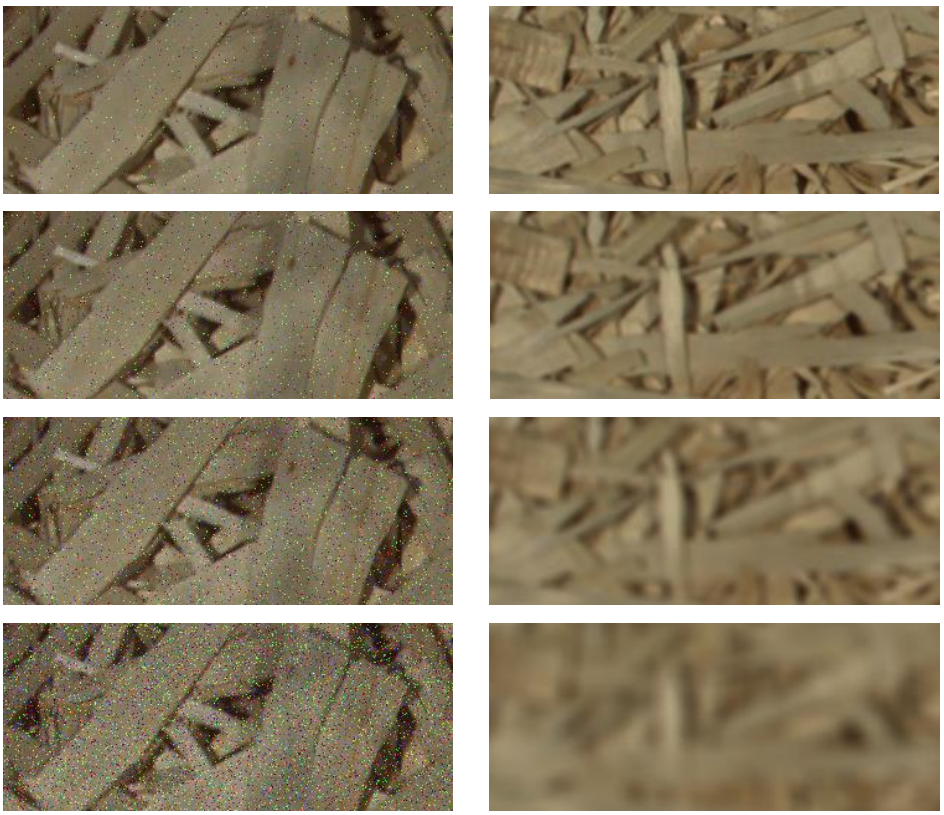

Figure 28 - Examples of the noisy images containing salt and pepper noise, which simulates device noise, (first column) and gaussian blur, which simulates the noise caused by a dirty lens or an out of focus problem, (second column).

The results obtained in a noisy environment are shown in Table 7. This table summarizes the results presenting the accuracy of the best k-NN model. With regard to salt and pepper noise, the system is capable of achieving an accuracy around 90%, even for images containing high-density noise. With regard to Gaussian blur, the results are also very satisfactory, since the accuracy is also greater than the 90% except for the highest noise, where, nonetheless, the results are still quite accurate. In general, these results show the robustness against noise of the approach based on frequency analysis.

	SALT AND PEPPER DENSITY					GAUSSIAN KERNEL$_{\text{STD DEV}}$			
NOISE	0.01	0.02	0.04	0.08		2_1	4_2	8_4	16_8
ACCURACY	92%	94%	92%	88%		94%	92%	92%	86%

Table 7 - Results obtained for noisy images.

4 CONCLUSIONS

This deliverable has presented the acquisition methods and image processing algorithm that have been developed to control the blending process.

The first method performs the granulometric analysis of falling wood strands, based on image processing techniques and three-dimensional reconstruction algorithms.

The method uses a specially-designed image acquisition setup, composed by two-cameras, and a specific acquisition procedure, designed for capturing the strands without motion blur effects, and with sufficient illumination. The method is able to compute a metric reconstruction of the particles, and estimate the size of the strands as they are falling, without control on the position and orientation of the strands during their fall. However, it is necessary that the strands fall inside the fields of view of the cameras.

The accuracy of the proposed method was evaluated by applying the method on a set of strands with different sizes, both compliant and non-compliant with the reference size provided by the manufacturing industry. The results exhibited a good accuracy, and showed the feasibility of the method. Moreover, results showed the possibility to use the method for determining when the size of the strands deviates from the reference size.

The second method captures 2-D images of the strands laid on a conveyor belt. Two different image processing approaches have been introduced to analyze these images.

One of them is capable of estimating the granulometry of the wood strands. The system uses an innovative approach based on the pyramidal segmentation of the images, which uses an optimized fuzzy color clustering to detect the wood strands and estimate their size. The method has been particularly developed to deal with the specific characteristics of the application. The performed experiments have also demonstrated that the system is suitable to detect changes in the granulometry that can deviate the optimal operation point specified for the factory.

The deliverable has also proposed a system able to estimate wood strand quality. This method is based on an innovative approach that avoids segmentation, a process that can be complex in industrial setups.

The method performs a quantization of the power spectrum of the Fourier transform, summarizing the energy contained in bands of one pixel. With this information, the system creates a histogram that is later exploited using a k-NN model. This model is used to predict the quality of the particles that appear in an image of the strands laid on a conveyor belt.

The performance of the system has been tested under different circumstances, obtaining good results that demonstrate its ability to analyze the quality of the strands and detect changes in it, even when the images contain a high degree of noise.

5 REFERENCES

[1] M. J. Thurley, "Automated online measurement of limestone particle size distributions using 3D range data," *Journal of Process Control,* vol. 21, no. 2, pp. 254-262, 2011.

[2] D. Slaughter, D. Giles and D. Downey, "Autonomous robotic weed control systems: A review," *Computers and Electronics in Agriculture,* vol. 61, no. 1, pp. 63-78, 2008.

[3] C.-J. Du and D.-W. Sun, "Recent developments in the applications of image processing techniques for food quality evaluation," *Trends in Food Science & Technology,* vol. 15, no. 5, pp. 230-249, 2004.

[4] T. Brosnan, "Inspection and grading of agricultural and food products by computer vision systems - a review," *Computers and Electronics in Agriculture,* vol. 36, no. 2-3, pp. 193-213, 2002.

[5] A. D. Switzer, "Measuring and Analyzing Particle Size in a Geomorphic Context," in *Treatise on Geomorphology*, Elsevier, 2013, pp. 224-242.

[6] K. Friedland, D. Ama-Abasi, M. Manning, L. Clarke, G. Kligys and R. Chambers, "Automated egg counting and sizing from scanned images: Rapid sample processing and large data volumes for fecundity estimates," *Journal of Sea Research,* vol. 54, no. 4, pp. 307-316, 2005.

[7] F. Ding, M. Benaoudia, P. Bédard, R. Lanouette, C. Lejeune and P. Gagné, "Wood chip physical quality definition and measurement," Pulp and Paper Laboratory, Centre de recherche industrielle du Qubec (CRIQ), Quebec, 2005.

[8] N. Theera-Umpon, E. R. Dougherty and P. D. Gader, "Non-homothetic granulometric mixing theory with application to blood cell counting," *Pattern Recognition,* vol. 34, no. 12, pp. 2547-2560, December 2001.

[9] V. Zapater, L. Martínez-Costa and G. Ayala, "A granulometric analysis of specular microscopy images of human corneal endothelia," *Computer Vision and Image Understanding,* vol. 97, no. 3, pp. 297-314, 2005.

[10] S. R. A. Iftikhar, A. Ali, M. Hussain and A. Jalil, "Capture Largest Included Circles: An Approach for Counting Red Blood Cells," in *Emerging Trends and Applications in Information Communication Technologies*, Springer Berlin Heidelberg, 2012, pp. 373-384.

[11] A. Boschetto and V. Giordano, "Powder sampling and characterization by digital image analysis," *Measurement,* vol. 45, no. 5, pp. 1023-1038, 2012.

[12] A. Mazzoli and O. Favoni, "Particle size, size distribution and morphological evaluation of airborne dust particles of diverse woods by Scanning Electron Microscopy and image processing program," *Powder Technology,* vol. 225, pp. 65-71, 2012.

[13] K. C. Williams, W. Chen, S. Weeger and T. J. Donohue, "Particle shape characterisation and its application to discrete element modelling," *Particuology,* vol. 12, pp. 80-89, 2014.

[14] M. Salehizadeh and M. Sadeghi, "Size distribution estimation of stone fragments via digital image processing," in *Advances in Visual Computing*, Springer, 2010, p. 329–338.

[15] T. K. Koh, N. Miles, S. Morgan and B. Hayes-Gill, "Image segmentation of overlapping particles in automatic size analysis using multi-flash imaging," in *Applications of Computer Vision, 2007. WACV'07. IEEE Workshop on*, 2007.

[16] R. L. Geimer and C. L. a. Link, "Flake classification by image analysis," U.S. Dept. of Agriculture, Forest Service, Forest Products Laboratory, 1988.

[17] T. Nishimura, J. Amin and M. P. Ansell, "Image analysis and bending properties of model osb panels as a function of strand distribution, shape and size," *Wood Science and Technology,* vol. 38, pp. 297-309, 2004.

[18] S. Ferrari, V. Piuri and F. Scotti, "Image processing for granulometry analysis via neural networks," in *IEEE International Conference on Computational Intelligence for Measurement Systems and Applications, CIMSA 2008*, 2008.

[19] A. Zadorozny, H. Zhang and M. Jagersand, "Granulometry using image transformation techniques," in *International Conference on Vision Interface*, 2002.

[20] A. Ledda, J. Quintelier, P. Samyn, P. D. Baets and W. Philips, "Quantitative image analysis with mathematical morphology," in *Proceedings of ProRISC 2003*, 2003.

[21] M. G. Ljungqvist, M. E. Nielsen, B. K. Ersbøll and S. Frosch, "Image Analysis of Pellet Size for a Control System in Industrial Feed Production," *PLoS ONE,* vol. 6, no. 10, p. e26492, 2011.

[22] M. Lopez, J. Vilan, J. Matias and J. Taboada, "Quality control of wood-pulp chips using a 3d laser scanner and functional pattern recognition," in *2007*, Proc. of the IEEE International Symposium on Industrial Electronics.

[23] M. Kempkes, T. Vetter and M. Mazzotti, "Measurement of 3D particle size distributions by stereoscopic imaging," *Chemical Engineering Science,* vol. 65, no. 4, pp. 1362-1373, 2010.

[24] I. Soppela, S. Airaksinen, J. Hatara, H. Rikknen, O. Antikainen, J. Yliruusi and N. Sandler, "Rapid particle size measurement using 3D surface imaging," *AAPS PharmSciTech,* vol. 12, no. 2, pp. 476-484, 2011.

[25] Z. Zhang, "A flexible new technique for camera calibration," *IEEE Trans. on Pattern Analysis and Machine Intelligence,* vol. 22, pp. 1330-1334, 2000.

[26] J. Heikkila and O. Silven, "A four-step camera calibration procedure with implicit image correction," in *Proc. of the 1997 Conf. on Computer Vision and Pattern Recognition (CVPR)* , San Juan, Puerto Rico, 1997.

[27] R. I. Hartley and A. Zisserman, Multiple View Geometry in Computer Vision, Cambridge University Press, 2004.

[28] R. D. Labati, A. Genovese, V. Piuri and F. Scotti, "Two-view contactless fingerprint acquisition systems: a case study for clay artworks," in *Proc. of the 2012 IEEE Workshop on Biometric Measurements and Systems for Security and Medical Applications (BioMS)*, Salerno, Italy, 2012.

[29] M. López, J. Matías, J. Vilán and J. Taboada, "Functional pattern recognition of 3d laser scanned images of wood-pulp chips," in Pattern Recognition and Image Analysis," in *Lecture Notes in Computer Science,*, vol. 4477, Springer Berlin Heidelberg, 2007, pp. 298-305.

[30] SICK, "Sick Ruler E series," [Online]. Available: https://www.mysick.com/ecat.aspx?go=FinderSearch&Cat=Row&At=Fa&Cult=English&FamilyID=369&Category=Produktfinder&Selections=40694.

[31] ISO-IEC, ISO 9276 - Representation of results of particle size analysis.

[32] J. Canny, "A computational approach to edge detection," *IEEE Transactions on Pattern Analysis and Machine Intelligence,* Vols. PAMI-8, no. 6, pp. 679-698, 1986.

[33] J. C. Bezdek, R. Ehrlich and W. Full, "FCM: The fuzzy c-means clustering algorithm," *Computers & Geosciences,* vol. 10, no. 23, pp. 191-203, 1984.

[34] N. Otsu, "A threshold selection method from gray-levelhistograms," *IEEE Transactions on Systems, Man and Cybernetics,* vol. 9, no. 1, 1979.

[35] R. C. Gonzalez, Digital image processing, Upper Saddle River, N.J.: Prentice Hall, 2002.

[36] N. S. Altman, "An introduction to kernel and nearest-neighbor nonparametric regression," *The American Statistician,* vol. 46, no. 3, pp. 175-185, 1992.

[37] M. J. Thurley, "Automated Image Segmentation and Analysis of Rock Piles in an Open-Pit Mine," in *Digital Image Computing: Techniques and Applications (DICTA), 2013 International Conference on*, 2013.

[38] I. Onederra, M. J. Thurley and A. Catalan, "Measuring blast fragmentation at Esperanza mine using high-resolution 3D laser scanning," *Mining Technology,* p. p. 1743286314Y.000, 2014.

[39] T. Andersson, M. J. Thurley and J. E. Carlson, "A machine vision system for estimation of size distributions by weight of limestone particles," *Minerals Engineering,* vol. 25, no. 1, pp. 38-46, 2012.